U.PORTO
FEUP FACULDADE DE ENGENHARIA UNIVERSIDADE DO PORTO

DEPARTAMENTO DE ENGENHARIA QUÍMICA

INTEGRATED MASTER IN CHEMICAL ENGINEERING 2020/2021

Gas separation via hydrate-based process: experimental, modelling, validation and optimization of a microscale HGtS unit for continuous carbon capture

A Master's dissertation

by

Francisco José Guimarães Figueiredo Dias

Developed within the course of dissertation

held in

CoLAB NET4CO2 - Network for a Sustainable CO2 Economy

Supervisor at FEUP: **Professor Doutor Ricardo Jorge Santos**

Supervisor at NET4CO2: **Doutor Marcelo Filipe Costa**

September 2021

To all my family that is here for me

and to those who wanted to be.

“na hora de pôr a mesa, éramos cinco”

José Luis Peixoto

Agradecimentos/Acknowledgments

Quero expressar os maiores agradecimentos a todos os que contrbuiram para a conclusão de mais uma importante etapa na minha vida e a mais importante do meu percurso académico.

Aos meu pais, José e Ana Maria, por me darem todos os meios, amor e apoio para poder chegar onde a vontade me levar. Aos meus irmãos, Ana Teresa e João, não só pela proximidade e amizade mas também por me fazerem querer melhorar a cada dia.

Aos meus amigos do MIEQ Ana Luísa Guedes, Beata Shymon, Inês Rodrigues, Sara Pestana, José de Sá, Rita Fernandes, Helder Fontes e Lígia Campos por me proporcionarem os melhores momentos durante esta etapa e estarem sempre lá nos menos bons.

Aos meus orientadores Professor Doutor Ricardo Santos e Doutor Marcelo Costa por me acompanharem durante esta etapa do meu percurso académico e por toda a sua disponibilidade e compreensão.

É também da maior importância salientar o esforço da NET4CO2, enquanto instituição, para me disponibilizar todas as condições para a realização deste trabalho, particularmente na situação pandémica que atravessámos. Um especial agradecimento ao Carlos Teixeira pela boa disposição, paciência e disponibilidade pois, sem ele, este trabalho nunca teria seria possível de realizar. Á Ana Rita Martinho e ao Gustavo Rangel pela ajuda e companheirismo.E a toda a equipa do NET4CO2 pela amabilidade com que me receberam. Todos eles tornaram a minha integração nesta empresa numa experiência muito gratificante.

O Doutor Ricardo Santos, orientador desta dissertação, é membro integrado do Laboratório Associado LSRE-LCM financiado por fundos nacionais através da FCT/MCTES (PIDDAC): Financiamento Base UIDB/50020/2020. O Doutor Ricardo Santos agradece ainda o financiamento do Projeto PTDC/EQU-EPQ/30445/2017 - POCI-01-0145-FEDER-030445 - financiado pelo Fundo Europeu de Desenvolvimento Regional (FEDER), através do COMPETE2020 – Programa Operacional Competitividade e Internacionalização (POCI) e com o apoio financeiro da FCT/MCTES através de fundos nacionais (PIDDAC).

Resumo

O presente trabalho concentra-se no arranque da mais recente unidade experimental da NET4CO2 de escala micrométrica, a P01, para operação em contínuo com vista à produção de hidratos de CO_2, como forma de separar gases de queima, através do recursso a reactores NETmix que são a peça central da unidade. Esta dissertação inclui estudos de transferência de calor e massa no NETmix assim como análise experimental do processo em contínuo de produção de hidratos de gás e análise de amostras obtidas.

Os testes de transferência de calor envolveram trocas de calor no NETmix com vista a determinar a capacidade da tecnologia de remover calor. Para estudar a transferência de massa foram injetados juntamente no reactor àgua e CO_2 sendo que a partir da quantidade de gás capaz de ser absorvido estimou-se o coeficiente associado à dissolussão de CO_2. A produção contínua de hidratos foi realizada para hidratos de CO_2 puros e de CO_2 com THF. Para várias experiências foram alterados caudais de àgua e de CO_2 assim como a pressão e concentração de THF, de forma a conhecer o impacto de cada um deste parametros na produção contínua de hidratos. Fez-se recolha de amostras obtidas a diferentes condições para estudar variações na composição do sólido obtido.

Foram realizados balanços energéticos aos reactores NETmix tendo sido obtidos coeficientes globais de transferência de calor entre os 200 e os 4000 $W \cdot m^{-2} \cdot {}^{o}C^{-1}$ demonstrando que a tecnologia apresenta maior capacidade de remover calor do que outras tecnologias que são aplicadas industrialmente. Testes de dissolução de CO_2 em àgua permitiram obter coeficentes volumétricos de transferência de massa entre os 2000 e os 6200 h^{-1} provando que a taxa a que a tecnologia dissolve gás em líquido é mais do triplo quando comparado com outras tecnologias com aptidão para este tipo de processos. Na produção de hidratos de gás só a pressão e concetração de THF tiveram um impacto visível tendo facilitado o iníco da formação de hidratos assim como a sua produção contínua. As amostras extraídas não revelaram susceptibilidade ás diferentes condições a que foram obtidas tendo sido a concentração de CO_2 em massa observada entre 13,3-14,3%.

Este trabalho mostra que a tecnologia NETmix é promissora para a produção em continua de hidratos de gás uma vez que revela qualidades importantes para esse processo: capacidade extrema para remover calor libertado durante processos exotérmicos e qualidade para dissolver grandes quantidades de gás numa fase líquida.

Palavras Chave: Hidratos, Transferência de calor, Transferência de massa, Produção contínua, NETmix, Dióxido de carbono

Abstract

This work focuses in the start up of the latest experimental unit of micrometre scale from NET4CO2, P01, that operates continuously in order to produce CO_2 hydratres, as a way of separating exhaust gases using Netmix reactors, which work as the central piece of the unit. This thesis includes studies of mass and heat transference in NETmix as well as experimental analysis of the continuous process of gas hydrates and the analysis of the collected samples.

The tests of heat transference involved heat exchange in NETmix so as to determine the technology's capacity of heat removal. In order to study mass transfer water and CO_2 were injected in the reactor and a coefficient related to the dissolution of CO_2 in water has been estimated from the quantity of gas which had been absorbed. The continuous production of hydrates has been conducted to hydrates of CO_2 pure and CO_2 with THF. In several experiments the water and CO_2 flow have been altered and so has the pressure and concentration of THF, as a way to learn about the impact of each of these parameters in the continuous production of hydrates. Samples obtained in different conditions have been collected to study variations in the composition of the resulting solid.

Energy balances have been conducted to the NETmix and global coefficients of heat transfer between 200 and 4000 $W \cdot m^{-2} \cdot {}^{o}C^{-1}$ have been recorded, thus showing that this technology presents a larger capacity for removing heat than other existing technologies used/employed by industries. Testing the dissolution of CO_2 in water has resulted in volumetric coefficients of mass transference between 2000 and 6200 h^{-1}, therefore proving that the rate at which this technology will dissolve gas in liquid triples when compared to other technologies that perform similar processes. In the production of gas hydrates only the pressure and concentration of THF have had a visible impact, which made the beginning of the formation of hydrates and the continuous production far easier. The samples obtained have not proven susceptible to the different conditions in which they have been collected, as they recorded a mass concentration of CO_2 varying between 13,3-14,3%.

This work demonstrates that NETmix is a promising technology to be considered in the continuous production of gas hydrates for it ensures fundamental qualities to this process: extreme capacity to remove the heat released during exothermic processes and outstanding ability to dissolve large quantities of gas in a liquid phase.

Key words: Hydrates. Heat Transference, Mass Transference, Continuous Production, NETmix, Carbon Dioxide

Declaration

I hereby declare, on my word of honour, that this work is original and that all non-original contributions were properly referenced by identifying the source.

Setember 20th 2021

Index

Figure List

Table List

Notation and Glosssary

A	Normal area	[m^2]
c_g	Concentration in gas	[$mol \cdot m^{-3}$]
c_L	Concentration in liquid	[$mol \cdot m^{-3}$]
c_g^i	Concentration in gas at the interface	[$mol \cdot m^{-3}$]
c_L^i	Concentration in liquid at the interface	[$mol \cdot m^{-3}$]
c_g^*	Concentration in gas in equilibrium with the liquid	[$mol \cdot m^{-3}$]
c_L^*	Concentration in liquid in equilibrium with the gas	[$mol \cdot m^{-3}$]
c_p	Specific heat	[$J \cdot kg^{-1} \cdot {}^oC^{-1}$]
d	Channel diameter	[mm]
d_h	Hydraulic diameter	[mm]
D	Chamber diameter	[mm]
h	Convective heat transfer coefficient	[$W \cdot m^{-2} \cdot {}^oC^{-1}$]
H	Equilibrium constant	
k	Thermal condutivity	[$W \cdot m^{-1} \cdot {}^oC^{-1}$]
k_La	Volumetric mass transfer coefficient	[h^{-1}]
l	Channel lenght	[mm]
n	Number of moles	[mol]
n_h	Hydration number	[$mol \cdot mol^{-1}$]
n_x	Number of rows	
n_x	Number of columns	
N	Dissolution rate	[$mol \cdot m^{-3} \cdot h^{-1}$]
Q	Mass flow rate	[$kg \cdot h^{-1}$]
$\dot{Q}$	Heat exhcanged	[W]
R	Resistance	[$m \cdot {}^oC \cdot W^{-1}$]
Re_c	Channel's Reynolds number	
S	Separation factor	
T	Temperature	[^oC]
T_{lm}	Logarithmic mean temperature	[^oC]
U	Overall heat transfer coefficient	[$W \cdot m^{-2} \cdot {}^oC^{-1}$]
V	Volume	[cm^3]
w	Network depth	[mm]

Greek letters

ΔT	Temperature difference	[^oC]
μ	viscosity	[Pa·s]
ρ	density	[$kg \cdot m^{-3}$]
$\bar{v}$	average velocity	[$m \cdot s^{-1}$]

List of Acronyms

BPR	Back Pressure Regulator
CCS	Carbon Capture and Storage
CSTR	Continuous Stirred Tank Reactor
FEUP	Faculdade de Engenharira da Universidade do Porto
GHG	Greenhouse Gases
HBCC	Hydrate-based Carbon Capture
HFC	Hydrofluorocarbons
HGtS	Hydra Gas to Solid
IGCC	Integrated Gasefication Combined Cycle
LPG	Liquified Petroleum Gas
MFC	Mass Flow Controller
PFC	Perfluorocarbons
TBAB	Tetrabutylammonium bromide
THF	Tetrahydrofuran

1 Introduction

Economic and population growth continue to be the most important drivers worldwide of increases in CO_2 emissions from fossil fuel combustion. Energy is the major driving-force for most economic activities around the world and fossil fuels are the primary resource for electricity required by modern society and will most likely remain in the foreseeable future. Even though the contribution of population growth between 2000 and 2010 remained roughly identical to the previous three decades, the contribution of economic growth on energy consumption has risen sharply[1].

As a consequence of the increase in energy consumption, the emission of pollutant gases to the atmosphere also increases. Greenhouse gases (GHGs) are of particular interest since their emissions highly contribute to climate change. Climate change is defined as the shift in climate patterns mainly caused by greenhouse gas emissions which cause heat to be trapped by the earth's atmosphere (greenhouse effect), and this has been the main driving force behind global warming. Each of the last four decades has been successively warmer than any decade that preceded it since 1850. According to the 2021 report of the International Panel on Climate Change, global surface temperature in the first two decades of the 21st century was 1.10°C higher than in the period 1850-1900[2].

The greenhouse gases widely discussed in the literature are carbon dioxide (CO_2), methane (CH_4), nitrous oxide (N_2O), and the fluorinated gases such as hydrofluorocarbons (HFCs), perfluorocarbons (PFCs) and sulphur hexafluoride (SF_6)[3]. According to the emissions gap report prepared by the United Nations Environment Programme in 2019[4], the total greenhouse gas emissions in 2018 amounted to 55.3 GtonCO_2e, of which 37.5 GtonCO_2e are attributed to fossil CO_2 emissions from thermoelectric power plants and industrial plants (such as steel mills and refineries).

Global warming caused by the greenhouse effect does not only affect the climate as it also endangers human life. In 2018 the world encountered 315 cases of natural disasters which are mainly related to climate change. Approximately 68.5 million people were affected, and economic losses amounted to $131.7 billion, of which storms, floods, wildfires and droughts accounted for approximately 93%. In 2018 alone economic losses attributed to wildfires in 2018 alone are almost equals collective losses from wildfires over the past decade[5], which is quite alarming. Although wildfires are part of the natural system, it is clear that human-induced emissions are directly interfering and amplifying the impact of natural system emissions. It is evident that human induced climate change is a major driving force behind many natural disasters occurring globally.

Being these planetary concerns, strict global regulations of CO_2 emissions to the atmosphere have been imposed. Various industries need to deal actively with these regulations in order to survive. It is by far evident that conventional mitigation efforts alone were not sufficient to meet the targets stipulated by the Paris agreement, therefore, the utilization of alternative routes appears inevitable. There is an urgent need to develop CO_2 reduction technologies, and carbon capture and storage (CCS) has great potential to be one of the more important green technologies in the future. Carbon capture from fossil fuel-burning power-generation plants will be a necessity if CCS is to make a material impact on total anthropogenic emissions[6]. It is also an area where the opportunity for a rapid reduction of emissions exists since some key technologies have been developed and deployed in other industries.

1.1 Motivation and Relevance

Several technologies for carbon capture already exist and can successfully separate carbon dioxide from gas mixtures. Unfortunately, all these technologies combine great energy consumption or require expensive materials or processes. The main motivation for this thesis is to assist NET4CO2 in the study of an hydrate gas to solid (HGtS) technology to separate CO_2 from exhaust gases, with basis on the PhD thesis by M.F.Costa (2017), that aims to tackle these main issues.

The Collaborative Laboratory NET4CO2, a private non-profit organization, is a network of Research & Development competences and technologies with the goal of creating new processes and products that make a significant contribution to the CO_2 sustainable circular economy.

The NET4CO2 aims to mitigate the trend of atmospheric CO_2 increase without compromising the quality of life we are used to. For that, technical solutions are being developed on two main fronts:

• A safe, efficient, and profitable capture and separation of CO_2.

• A competitive production of alternative fuels: synthetic fuels, which provide a route for CO_2 and CH4 reutilization; and hydrogen which involves zero CO_2 emissions.

NET4CO2 has already produced gas hydrates using NETmix reactors at a lab scale (1 $kg \cdot h^{-1}$) and pilot scale (10 $kg \cdot h^{-1}$). A main goal for the Colaborative Laboratory NET4CO2 is to produce, in a near future, 1 $ton \cdot h^{-1}$ of hydrates which will be a great step to bringing this technology closer to be implemented in industrial processes.

1.2 Thesis Objective and Structure

The main objective of this work is to initiate the studies on a new microscale unit, called P01, for continuous hydrate formation and gas separation that has a microNETmix reactor as its central piece, as well as measuring its capabilities and testing its features.

The present thesis is divided as follows:
In Chapter 1 the motivation and relevance of the present work is provided, as well as the main objectives.

In Chapter 2 a global overview of the main problem involved is presented. The necessity of mitigating CO2 emissions is stated as well as the fundamental role of CCS technologies for this purpose. The fundamentals of the CO_2 capture process, transport and storage are detailed. The available capture technologies are explained with special attention to hydrate-based capture. Gas hydrates are defined and fundamentals for its formation and previous works regarding CO_2 hydrates are discussed. The NETmix technology is described as well as the available prototypes. Previous works and applications of this technology are introduced.

In Chapter 3 the material and methods applied in this work are described. The materials used are specified. The experimental unit P01 is presented as well as some of its features. Its process flow diagram is thoroughly described, and special attention is given to the unit's central piece, the NETmix reactor. The experimental procedure for each following chapter is provided.

Chapter 4 introduces heat transfer and heat transfer coefficients and the heat performance of the NETmix is presented.

Chapter 5 provides some theoretical background to mass transfer between phases and presents an evaluation of the NETmix ability to dissolve CO_2 in water.

Chapter 6 is divided in two parts, the former where continuous CO_2 and CO_2+THF hydrate production is carried out and the latter where samples of the hydrate produced are subjected to a gravimetric analysis.

Chapter 7 presents the main conclusions of the present work as well as suggestions for the continuation of studies on this topic.

1.3 Main difficulties

Although a great deal of practical work is described in this thesis, a lot of setbacks had to be dealt with during the period of experimental tests. For once, it started during the initial lockdown phase which required some time to the student and CoLab to adapt to the situation. Health issues due to the Covid-19 pandemic interrupted the practical work for a great deal of

time, requiring the pace at which the tests presented in this thesis were performed to accelerate.

Also, a great deal of work performed is not suited to be presented in this dissertation. Since the experimental unit was new and not tested before a lot of repairing, tuning and equipment change was required until each experiment was able to be carried out. This extra work required not only manual work to fix leakages or substitute tubes and main equipment such as a heat exchanger and a chiller, but also theoretical background to support the changes in the unit that were successively carried out.

2 State of the Art

2.1 Carbon Capture and Storage

Rapid economic growth has contributed to today's ever-increasing demand for energy. An obvious consequence of this is an increase in the use of fuels, particularly conventional fossil fuels.

The abundant use of fossil fuels has become a cause of concern due to adverse effects on the environment, particularly related to the emission of carbon dioxide (CO_2), a major greenhouse gas (GHG)[7]. Figure 2.1 shows the annual emission of anthropogenic GHG between 1970 and 2010. In 2011, according to the Emission Database for Global Atmospheric Research, CO_2 global emissions reached 33.4 billion tonnes, which is 48% higher than two decades ago[8].

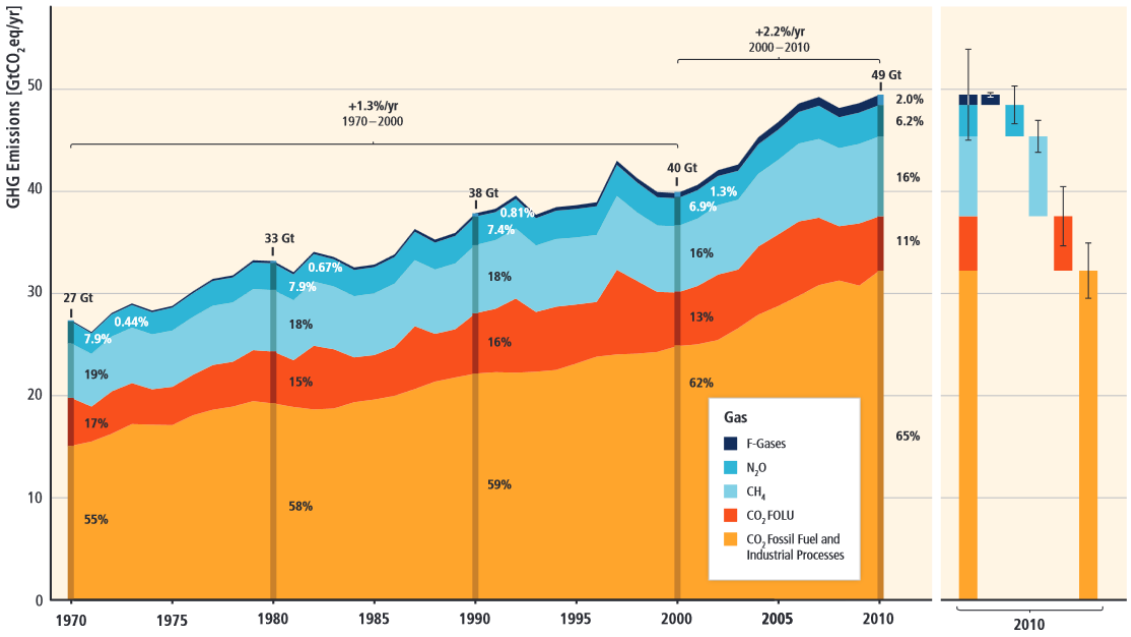

Figure 2.1: Total annual anthropogenic GHG emissions (GtCO2eq/yr) by groups of gases 1970 - 2010 (IPCC, 2014)

To reduce their emissions, different approaches are being considered and adopted by different countries, such as[9]:

- Improving energy efficiency and promoting energy conservation;
- Increasing usage of low carbon fuels, including natural gas, hydrogen or nuclear power;
- Deploying renewable energy, such as solar, wind, hydropower and bioenergy;
- Applying geoengineering approaches such as afforestation and reforestation;

Despite the fact that these measures prove to be an important step towards mitigation of the release of GHG to the atmosphere, these do not act directly on the source of CO_2 emissions. At

the same time research and development efforts into low- or zero carbon alternatives to fossil fuels are carried out, the urgent need to stabilize anthropogenic CO_2 levels means that measures such as the capture and storage of carbon, that would otherwise be emitted, might play an important role during the period of transition to low-carbon alternatives.

Carbon capture and storage (CCS) is a promising route significantly replace the amount of CO_2 emitted to the atmosphere, via the use of fossil fuels without changing neither industrial processes nor their efficiency, that could arise from the change of the energy source[10].

CCS can reduce the amount of CO_2 emissions, not only from power generation, but also from industrial sectors, such as iron and steel, refining, petrochemical or cement manufacturing[11], and is estimated to be able to provide almost 20% of global emission cuts required by 2050.

2.2 Capture Process

The fundamental chemical process involved in the generation of power from carbon-based fuel is the exothermic oxidation of carbon, and since CO_2 is the lowest-energy endpoint of the oxidative reaction chain its production is unavoidable. The elimination of carbon from power plant emissions therefore requires either[12]**:**

- Decarbonation of the fuel prior to combustion (pre-combustion capture)
- Separation of CO_2 from the products of combustion (post-combustion capture)
- Reengineering the combustion process to produce CO_2 as a pure combustion product (oxyfuel combustion)

A simple description of each process for carbon capture is described in Figure 2.3.

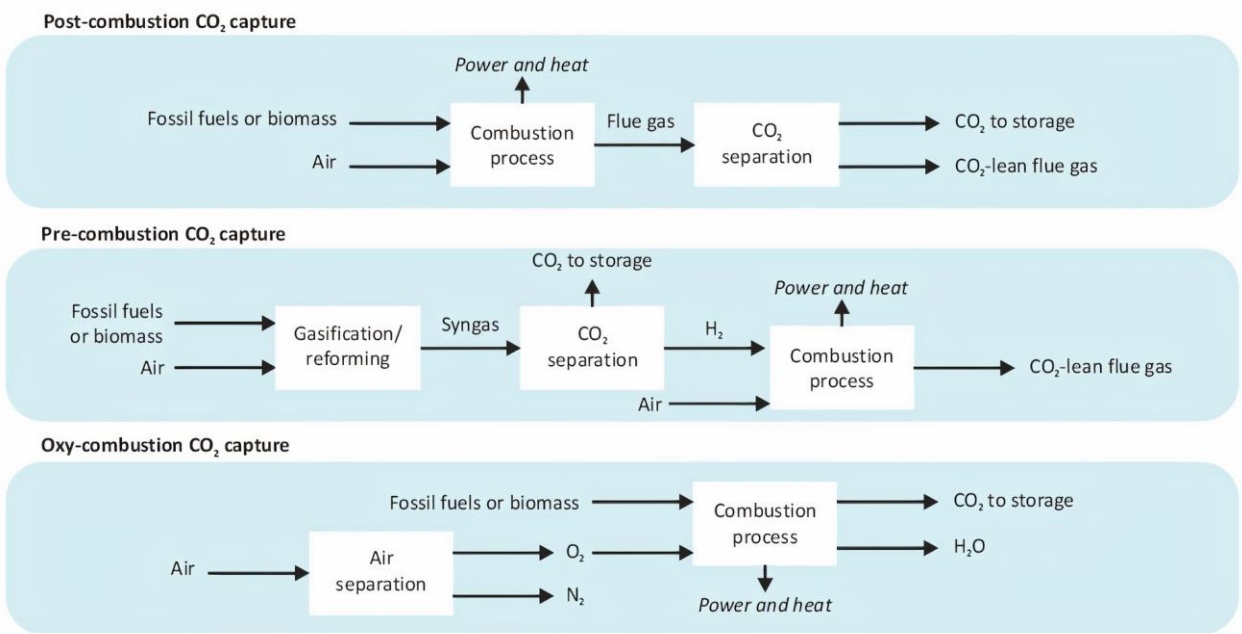

Figure 2.3: CO_2 capture processe. Source: [9]

2.2.1 Pre-Combustion

Pre-combustion capture involves decarbonation by gasification of the primary fuel (typically coal or natural gas) to produce hydrogen through a combination of partial combustion, reforming and water–gas shifting, and the separation of CO_2 from the resulting product stream[11].

In this process, an initial reaction stage where syngas (a mixture of hydrogen, carbon monoxide and carbon dioxide) can be obtained either via oxidation by adding oxygen or air, or steam reforming by adding steam. After each of these reactions, the syngas is mixed with more steam, in a catalytic reactor, to obtain more hydrogen and further reduction of CO to CO_2[13]. The result is a H_2/CO_2 flue gas with a CO_2 concentration over 20%.

2.2.2 Post-combustion

In post-combustion capture, CO_2 is removed from the combustion reaction product stream – the flue gases – immediately before they enter the stack. Instead of being discharged directly to the atmosphere, flue gas is passed through equipment which separates most of the CO_2. In this sense, it is thus an extension of the flue gas treatment for sulphur dioxide (SO_2), nitrogen oxides (NOx), or particulate control on an existing facility, made more challenging since the CO_2 level in combustion flue gas is normally quite low (i.e.7–14% for coal-fired and as low as 4% for gas-fired). The flue gas that reaches the capture system is a mixture of mostly nitrogen and carbon dioxide, with traces of water vapour, resulting from the combustion with air[9,12,14].

The advantage of this approach is that it would allow retrofit at existing facilities that can accommodate the necessary capturing hardware and ancillary equipment without having to modify the plant itself[15]. For this reason, post-combustion capture is often the preferred economic solution, especially for older power plants.

2.2.3 Oxyfuel combustion

In oxyfuel combustion, oxygen instead of air is used for combustion. This reduces the amount of nitrogen and thermal NOx and its compounds, such as NO and NO_2, present in the exhaust gas that would affect the subsequent separation process[16].

The exhaust gas is then composed mainly by CO_2, water vapour, particulate matter and SO_2[17]. After removing particles and SOx the flue gas will contain a CO_2 concentration ranging from 80% to 98 %, depending on the burnt fuel. However, the large oxygen consumption, coming from an energy intensive air separation unit, results in high cost and the energy consumption increase may reach over 7% when compared with a plant without CCS.

2.2.4 Transport

The large-scale deployment of CCS will require the development of a transportation infrastructure to interconnect capture and storage sites. While road and rail transport have been used at a smaller scale, pipeline and marine transport are the only realistic options for transporting quantities big enough to have an impact on global CO_2 emissions.

The technology for pipeline and marine transport is already well developed for transport of liquefied petroleum gas (LPG). Carbon dioxide can be transported in the same way, but at smaller scales due to its limited demand[17].

2.2.5 Storage

Once captured, CO_2 is compressed and shipped or transported via pipeline, to be stored either in the ground, ocean or as a mineral carbonate[17]. The main concerns with CO_2 storage and feasibility of storage sites include the distance from CO_2 source, effective storage capacity, economic constraints, possible leaks, and the related damage that a concentrated CO_2 stream would cause if it escaped into the environment.

CO_2 injection into permeable rock formations - geological storage – is, to date, the only method of carbon storage that has been applied at a commercial scale, probably presenting as one of the most promising and viable options for storing the quantities needed to effectively reduce global warming and related climate change. There is growing confidence in trapping CO_2 in deep saline aquifers and oil or gas reservoirs since natural gas has been trapped in these geological formations for millions of years by some of the very same mechanisms that are known to trap CO_2[9].

2.3 Capture Technologies

Many chemical and physical CO_2 extraction methods are widely studied and available and, although carbon capture can represent an important step towards CO_2 mitigation, the cons of using those technologies withhold the industrial system from implementing them. A list of separation techniques and processes, including its advantages, is presented in Table 2.1.

Table 2.1: Advantages and disadvantages for existing CO_2 capture technologies. Source: [20]

Type	*Advantages*	*Disadvantages*
Membranes	Capture efficiencies can achieve more than 90% in multi-stage systems Work continuously and at ambient temperatures Do not require additional chemicals Relatively low installation costs	Huge energy penalties Depending on the process, active deposits can be frequent, affecting efficiency
Absorption	Most mature process for CO2 separation High separation efficiencies (>90%)	Separation efficiencies are dependent on CO_2 concentration Significant amounts of heat for absorbent degradation are required Environmental impacts related to absorbent degradation need to be better understood
Adsorption	Capture efficiencies from 85% to 90% CO2 purity can achieve 95% in some processes Possible hydrogenation co-production	Energy penalties and costs are still not competitive
Chemical Looping Combustion	Avoids energy intensive air separation processes	There are no large-scale operations Impossibility of retrofitting existing power plants
Calcium Looping	Energy penalties are competitive with other technologies It provides the possibility for a co-production of syngas	Underdeveloped technique
Cryogenic	CO_2 can be captured in different phases and so, and additional compression stage can be avoided Possibility for recovering high purity CO2 which is more valuable for the industrial market	The required energy consumption for cooling can increase energy penalties Some technologies performance is highly dependent on flue gas conditions

2.3.1 Hydrate Based Capture

Hydrate-based carbon capture (HBCC) technologies have been receiving increasing attention due to its unique separation mechanism and formation under the favourable thermodynamic conditions of low temperature and high pressure. Even though hydrates have been studied since 1934 when Hammerschmidt found its formation in pipelines transporting gas, this technique has not been given much attention for carbon capture purposes.

Post-combustion CO_2 capture separates CO_2 from the flue gas at the downstream of fuel combustion, which consists of approximately 15-20% CO_2 and 79-80% N_2. In pre-combustion

processes such as integrated gasification combined cycles (IGCC), CO_2 capture separates CO_2 from the CO_2/H_2 syngas, which consists approximately 40% CO_2 and 60% H_2. As shown in Table 2.2, CO_2 has the lowest hydrate-forming pressure in comparison with the other mixed components in exhaust gases[21].

Table 2.2: Generation of various gas hydrates at 273K. Source: [15]

Gas	H_2	N_2	CH_4	O_2	CO_2
P / MPa	231	16,3	2,65	11,1	1,22

This means CO_2 is easier to form hydrate thus enabling the separation from the other gases in the mixture and trapping CO_2 molecules in a solid phase that will be enriched with that component. The CO_2 hydrate can be later dissociated by depressurization and/or heating[23].

Compared with other CO_2 capture methods, HBCC process is free of contamination as water is the raw material. Besides, one volume of CO_2 hydrate can hold as much as 160 volumes of CO_2 (when compared to gaseous CO_2 at PTN conditions) which makes this method a potential way to transport and store CO_2[22]. This technology seems very promising for carbon capture and storage since it can be proven useful in all its stages: capture, transport, and geological storage.

2.4 Gas Hydrates

Gas hydrates are non-stoichiometric solid crystalline compounds where gas molecules (guests), such as light hydrocarbons or air components, are trapped in water cage-like networks (host) that are composed from hydrogen-bonded water molecules. Gas hydrates are a subset of compounds known as clathrates or inclusion compounds, which are formed under conditions of low temperature and high pressure. The hydrogen bonds cause the water molecules to align in regular orientation to which certain compounds connect by weak Van der Waals force causing the aligned molecules to stabilize and a solid mixture precipitates[24,25].

Hydrates are classified by the arrangement of the water molecules in the crystal, and hence the crystal structure. There are plenty of structures, but the three common natural structures of gas clathrate hydrate are: cubic structure I (sI), cubic structure II (sII) and, although less common, hexagonal structure H (sH)[26]. The properties each are described in Table 2.3.

The structure obtained is directly related to the guest molecule size, as each of these structures own different arrangements and number of the water molecules, resulting in different number and size of cavities available to host the guest gas molecules.

Table 2.3: Gas hydrates structural properties (Costa, 2017)

STRUCTURE	sI		sII		sH		
CAVITY TYPE	Small	Large	Small	Large	Small	Medium	Large
LABEL	5^{12}	$5^{12}6^2$	5^{12}	$5^{12}6^4$	5^{12}	$4^35^66^3$	$5^{12}6^8$
NUM. CAVITIES	2	6	16	8	3	2	1
AVERAGE CAGE RADIUS (Å)	3.95	4.33	3.91	4.73	3.94	4.04	5.79
COORDINATION NUMBER	20	24	20	28	20	20	36
LATTICE SIZE (Å)	12		17.3		12.2		
NUM. WATER MOLECULES	46		136		34		

2.4.1 Hydrate Formation

Hydrates are formed when free water is in contact with a hydrate-forming guest molecule, in temperature and pressure conditions that are thermodynamically favourable. An example of the range of conditions that need to be met for different gases are the hydrate phase equilibria for N_2/CO_2 represented in Figure 2.4. Hydrates formation should be treated as a crystallization process and although it is not a chemical reaction, for there is no creation or destruction of chemical bonds, it can be conceptualized as a reaction[24]:

$$\mathrm{G} + n_h \mathrm{H_2}O \leftrightarrow \mathrm{G} \cdot n_h \mathrm{H_2O} \tag{1.1}$$

Where n_h is the amount of water per guest molecule. Considering these are non-stoichiometric materials, as $n_\mathrm{h}$is not necessarily integer and varies for each guest molecules. The value of n_h can be determined considering the number of water molecules and the number of cavities occupied by the guest molecules. In the case of CO_2, the formed type I hydrate only has its large cavities filled, since the guest molecule is too large to fit in the smaller cages. Therefore, in theory only 6 molecules of carbon dioxide are encapsulated in the hydrate, leading to the following theoretical hydration number[10]:

$$n_\mathrm{h} = \frac{n_{\mathrm{H_2O}}}{n_{\mathrm{CO_2}}} = \frac{46}{6} = 7.66 \tag{1.2}$$

Hydrate formation requires supersaturating conditions of the aqueous medium, which means that the concentration of guest compounds must be higher than their solubility in water for the crystallization process to occur. If the amount of gas is higher than the saturation

concentration, the solution enters a second phase called nucleation, which is the phase where the nuclei of hydrates are being formed but still not visible[26]. Thus, nucleation is a process based on supersaturation and on its driving force, which is how favourable pressure and temperature are in comparison with the equilibrium conditions.

The next stage, hydrate growth, occurs when most of the gas is consumed, and as a result, interphase mass transfer from the gas phase to the liquid phase is of great importance. Both gas dissolution and hydrate formation (nucleation and growth) processes are highly exothermal processes, requiring high rates of continuous heat removal. When nucleation and growth occurs at a system unable to remove the released heat from the hydration process, then the heat is absorbed by the system's medium, and the temperature increases up to values where hydrates are not thermodynamically stable. Kang et al. (2001) made a comparison between enthalpies of dissociation of pure CO_2 and N_2 hydrate obtaining values of 65.2 and 65.8 $kJ \cdot mol^{-1}$, respectively[27].

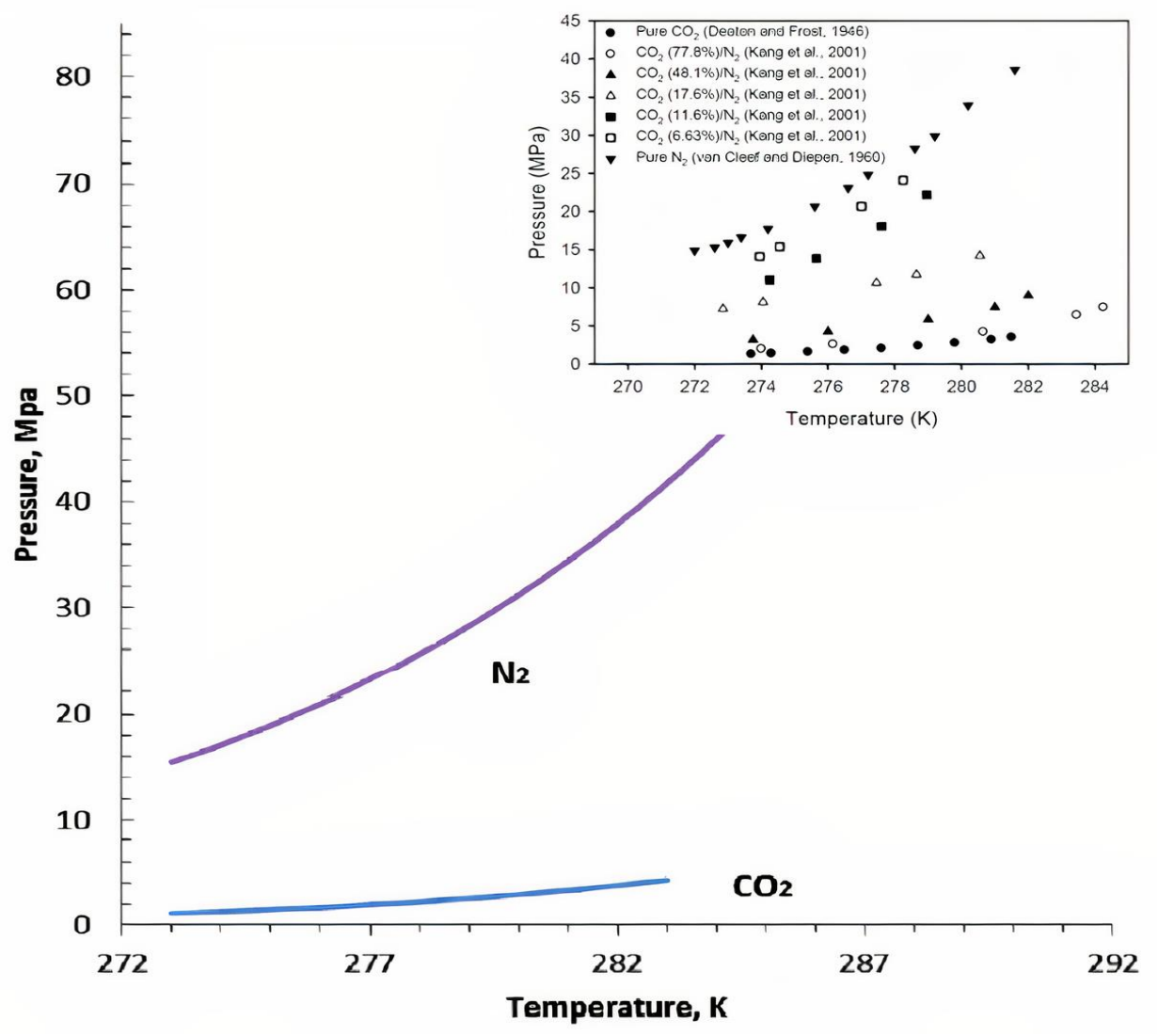

Figure 2.4: Hydrate equilibrium conditions for CO_2, N_2 and CO_2/N_2 mixtures hydrate formation.
Source: [28,29]

2.4.2 Chemical Additives

Chemical additives act as hydrate promoters that can reduce the equilibrium hydrate formation pressure, shorten the induction time, increase the hydration rate, enhance gas uptake or improve the selectivity of CO_2 in hydrate cages. These additives are generally divided into two classes: kinetic promoters and thermodynamic promoters. While kinetic promoters increase the rate of hydrate formation, by possibly increasing the gas dissolution rate in water, without taking part in the hydrate formation itself, thermodynamic promoters are small molecules that take part in the construction of structures enhancing their stabilization at moderate conditions of temperature and pressure[10,20,30].

The most tested thermodynamic promoters for HBCC are TBAB (tetra-n-butyl ammonium bromide) and THF (tetrahydrofuran). Kang et al. (2001) studied the influence of THF (tetrahydrofuran) in the CO_2/N_2 mixed system, determining the hydration number and the dissociation enthalpy. They observed a shift in the hydrate structure from I to II, which increased the amount of guest species. However, the increase in water molecules on the hydrate formed led to lower hydration numbers and the dissociation enthalpy increased by a factor of 2, with just 1% THF. Further understanding on the shifts in the hydration heat can be obtained by observing figure 2.5.

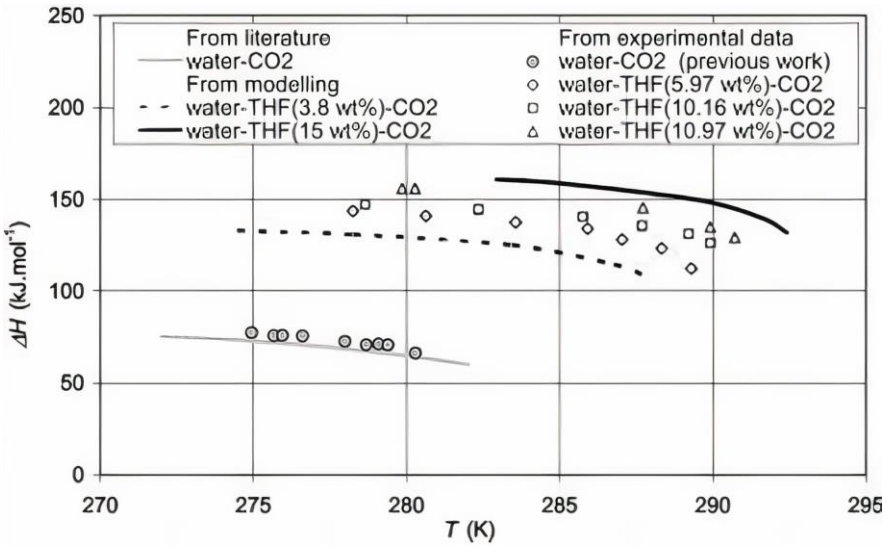

Figure 2.5: CO2 hydrates dissociation enthalpy and the effect of THF [31]

Linga et al. also studied the addition of THF to a CO_2/N_2 flue gas mixture observing the same shift in hydrate structure from sI to sII and lower hydrate formation pressure[32,33]. Nevertheless, although induction time and operating pressure were reduced, and CO_2 recovery rate increased to about 60%, THF molecules compete with CO_2 for large cavities, and thus, could not improve gas consumption and CO_2 separation factor[34] described in equation 1.3.

$$S = \frac{C_{CO_2}^H / C_{CO_2}^G}{C_{N_2}^H / C_{N_2}^G} \quad (1.3)$$

Where $C_{CO_2}^H$ and $C_{CO_2}^G$ are the concentration of CO_2 in the hydrate phase and gas phase, respectively and $C_{N_2}^H$ and $C_{N_2}^G$ are the concentration of mixed gas without CO_2 in the hydrate phase and gas phase, respectively.

Regarding other promoters it is claimed that CO_2 gas uptake in hydrates is larger when using THF than TBAB or others, hence making them a less viable option for carbon separation and capture.

2.4.3 Hydrate Production

Hydrates are rarely produced in high quantities since most processes developed are batch processes, such as stirred tank reactors or fixed bed crystallisers[25]. In stirred tank reactors, agglomeration of crystals may occur, reducing hydrate formation rate[34]. Fixed bed crystallisers have been studied as an alternative to overcome this problem, and although it allows the reduction of energy consumption and CO_2 recovery, it still remains as a batch process, being hard to continuously replicate the process. Using silica as a focus of crystallization has proved advantageous since its porous nature promotes the contact between water and gas, eliminating the need for intensive mechanical agitation and water excess. These technologies have the advantage of small energy penalty (6–8%)[8].

With all the advantages found in carbon capture via hydrate, the great challenge that is posed is to find or develop a piece of equipment capable of giving the water-gas mixture the intensive mixing it requires while being capable of removing heat at high rates and operating continuously.

2.5 The NETmix Technology

The NETmix is a new patented mixing technology (Lopes et al.,2005) consisting of a network of static mixing chambers interconnected by transport channels. Networks are formed by the repetition of unit cells, each unit cell consisting of one chamber and two inlet, and two outlet half-channels oriented at a 45° angle from the main flow direction. These cells can either be constructed from cylindrical chambers and rectangular cross section area channels or from spherical chambers and cylindrical channels[35]. All of the above mentioned features from the network arrangement to the channels and chambers structures can be observed in Figure 2.6.

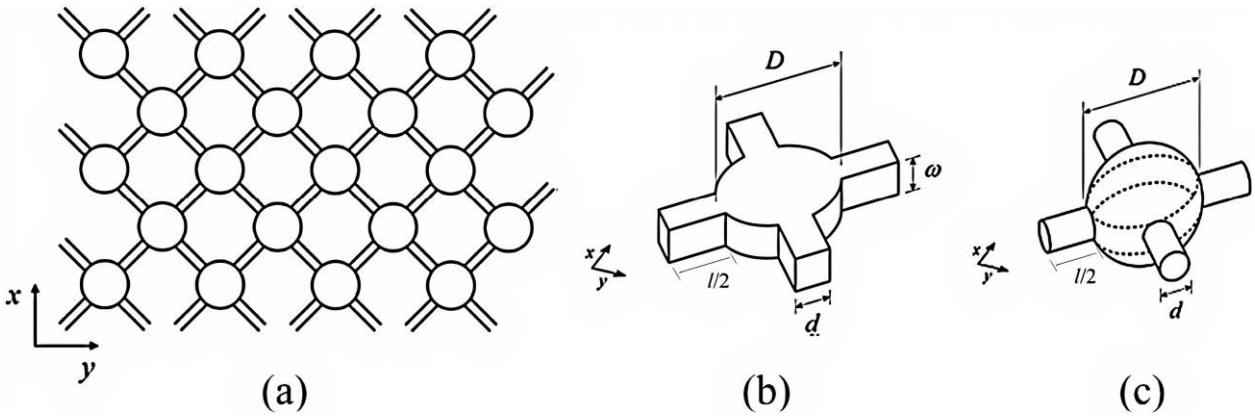

Figure 2.6: (a) NETmix network arrangement, (b) NETmix 2D channels and chambers and (c) NETmix 3D channels and chambers. Source: [36]

Mixing in the NETmix reactor can only be achieved above a critical channel's Reynolds number, of about 150, where the flow inside the mixing chambers evolves to a self-sustained oscillatory laminar flow regime that induces strong local laminar mixing[37], as demonstrated in Figure 2.7. This occurs due to the geometric characteristics of the NETmix network, as well as the local hydrodynamic instabilities induced by the jet's interactions at the chambers, and, therefore, no mechanical mixing equipment is present.

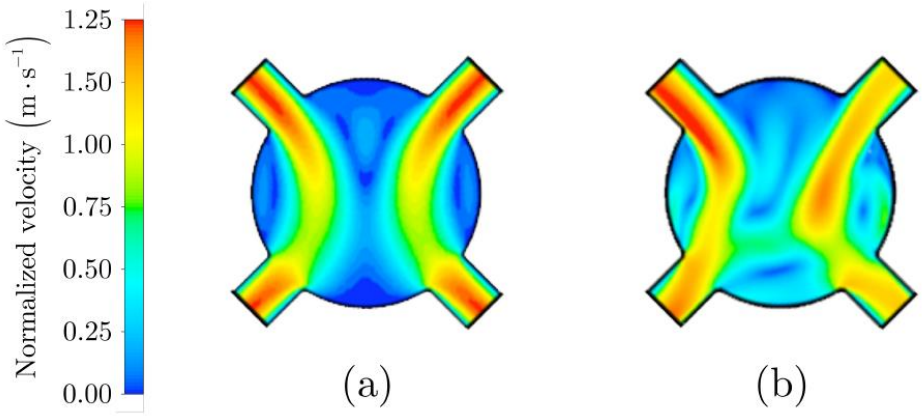

Figure 2.7: Velocity magnitude contour maps of NETmix chambers for (a) Re_c=70 (below critical Reynols number) and (b) Re_c=500 (above critical Reynols number). Source: [10], Adapted from: [38]

The channel's Reynolds number is defined by

$$\mathrm{Re_c} = \frac{\rho \bar{v_c} d_h}{\mu} \tag{1.4}$$

where ρ and μ are the fluid's density and viscosity, respectively, $\bar{v_c}$ is the mean channel's velocity and d_h is the channel's hydraulic diameter.

Channels can be conceptualized as plug flow reactors and chambers as continuous stirred tank reactors (CSTR), offering versatility to a wide range of chemical and physical processes. The difference from stirred tanks and NETmix is further accentuated when coupling the specific surface area and the heat transfer coefficient, resulting in about five orders of magnitude larger in some conditions. Previous works have shown NETmix is capable of removing heat at a rate that is almost one order of magnitude larger than microreactors (see Figure 2.8), due to laminar mixing induced by oscillations. In microreactors, the flow is parallel, and mixing is mostly achieved by molecular diffusion, because of the low convection rates that are observed, which leads to smaller heat transfer coefficients[10].

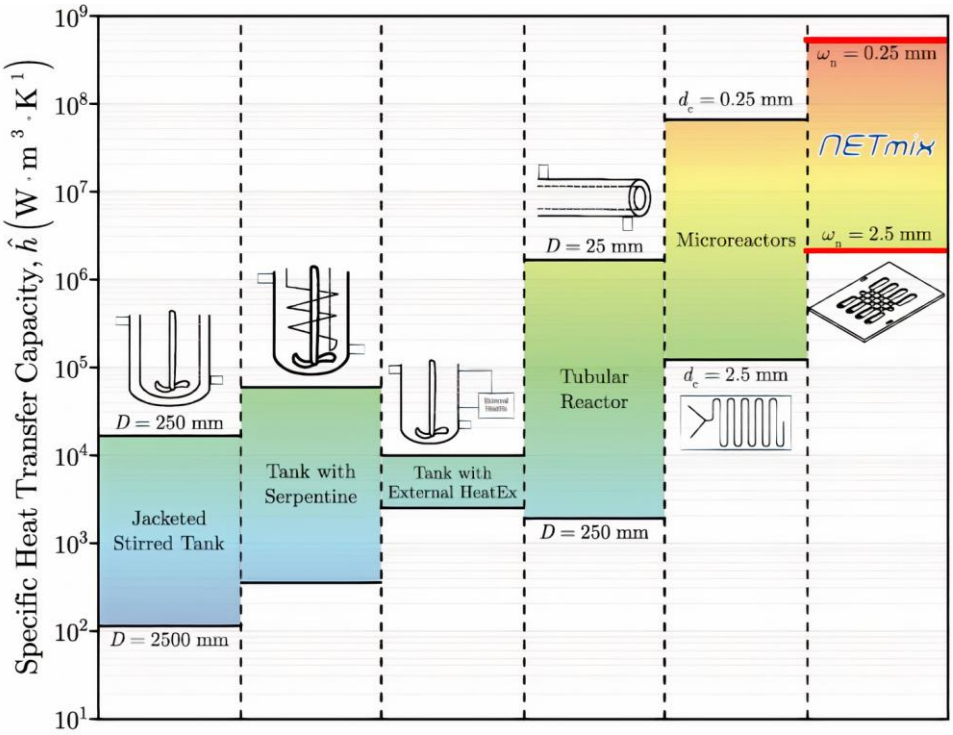

Figure 2.8: Specific heat transfer capacity comparison between typical heat exchange devices and NETmix. (Costa, 2017)

2.5.1 Existing Prototypes

Three different NETmix prototypes currently exist, which were built for different purposes. NETmix 3D (Figure 2.9a) was the first prototype ever built (Laranjeira, 2005) and had spherical chambers and cylindrical channels. NETmix 3D was constructed from two acrylic slabs where half chambers and channels were imprinted and then glued together.

The transition to the 2D configuration was introduced by Gomes (2011) and represents a considerable decrease in the construction complexity since only one of the slabs has the chambers and channels imprinted. The Lab-scale NETmix 2D (Figure 2.9b) is a small lab-scale unit and was built for research projects with small throughputs. For larger throughputs, the

Multi-Inlet NETmix 2D (Figure 2.9c) has the particularity of incorporating multiple inlet injection points along the reactor.

The geometrical characteristics of the NETmix 3D and the two 2D NETmix reactors are summarized in Table 2.4.

Table 2.4: NETmix 3D, Lab-scale NETmix 2D and Multi-Inlet NETmi 2D geomethrical characteristics. Source: [37]

Parameter	*Unit*			
		NETmix 3D	Lab-scale NETmix 2D	Multi-Inlet NETmix 2D
Number of rows, n_x	-	49	29	65
Number of columns, n_y	-	15	8	16
Chamber diameter, *D*	mm	7	6,5	8,75
Channel diameter, *d*	mm	1,5	1	1,5
Network depth, *w*	mm	-	3	5,9
Channel length, *l*	mm	3,2	2,1	5,4
Network volume, *V*	mL	140	23	1500

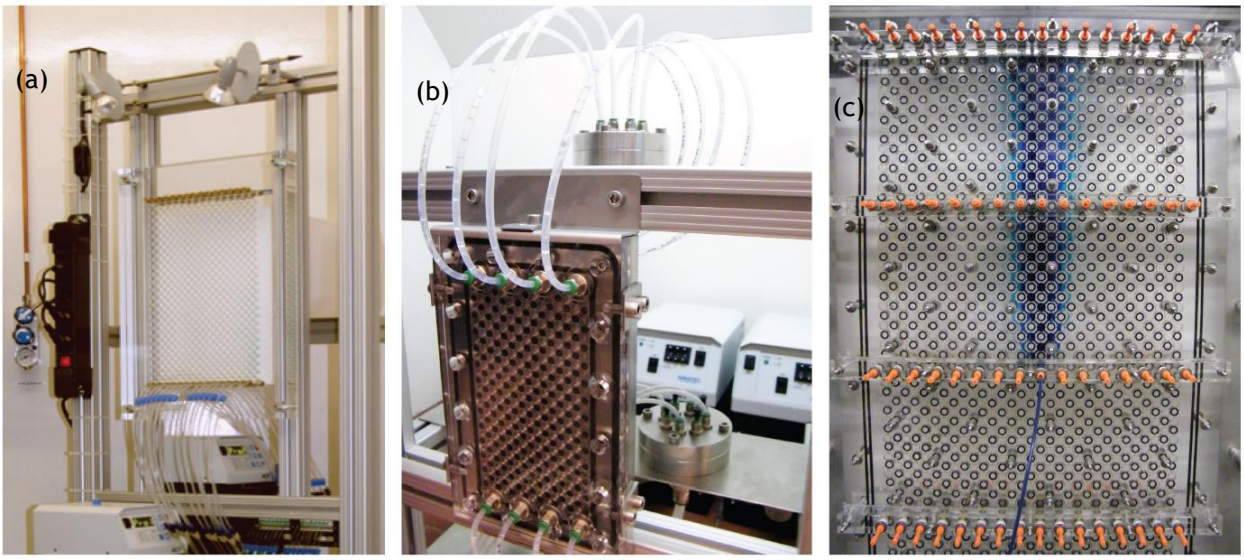

Figure 2.9: NETmix prototypes: a) NETmix 3D; b) Lab-scale NETmix 2D; c) Multi-Inlet NETmix 2D. (Fonte,2013)

2.5.2 Application of the NETmix Technology

NETmix network plates prove extremely useful to a wide range of activities from material production to separation processes.

A NETmix industrial reactor was developed by Fluidinova, a spin-off company from LSRE (Laboratory of Separation and Reaction Engineering) at FEUP (Faculdade de Engenharia da Universidade do Porto), to produce nanocrystalline hydroxyapatite materials, a biocompatible material that can act as bone or dental fillers, substitutes, or replacements. The advantage of using the NETmix for this process is due to the NETmix demonstrated capacity to produce

nanoparticles without the need of thermal or mechanical treatments, which allows relatively small particles to be created, as a result of the chaotic and oscillatory flow regime that is observed.

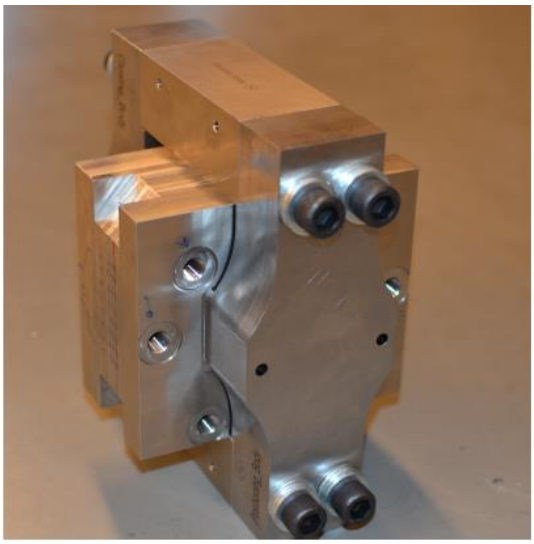

Figure 2.10: Assembled microNETmix reactor. (Costa,2017)

The microNETmix unit showed above in Figure 2.10 was used in FEUP to continuously produce CO_2 hydrates by M.F.Costa (2017). It is expected that hydrates nucleation and growth occurs at larger rates using the NETmix technology, when compared to stirred tanks, since mixing and both heat and mass transfer are enhanced, thus reducing transport resistances that are the limiting steps in crystallization kinetics and assuring the continuous slurry flow in the reactor[39].

Most recently, a mesostructured NETmix reactor was assembled for Laboratory of Separation and Reaction Engineering – Laboratory of Catalysis and Materials (LSRE-LCM) at FEUP to continuously produce hydroxyapatite Pickering emulsions. In order to achieve the industrial implementation of Pickering emulsions, continuous production and less intensive energy devices are required, and this is why the NETmix was chosen for it provides the ideal characteristics needed. Also, the local hydrodynamic instabilities induced by the immerging jet interactions at the chambers induces successive repeated and well-localized mixing inside the chambers throughout the reactor, which promotes an easily reproducible emulsification step[40].

In all the previously described applications, NETmix presents itself as a competitive advantage to both batch processes since the network can be easily scaled-up or numbered-up depending on the process and production objectives. Furthermore, it has already proven to efficiently handle multiphase and fast reactions, having unique capabilities to transport both mass and heat to and from the system (Gomes 2011, Fonte 2013), and other heat transfer-limited continuous processes.

3 Materials and Methods

3.1 Materials

Hydrate production for carbon capture requires water and CO_2. Gaseous carbon dioxide with a purity of 99.995% and water concentration below 20 ppm was supplied by Air Liquide (Alphagaz™ CO2) in bottles at approximately 60 bar. Tap water was supplied by Águas do Porto, E.M., with pH ranging from 6.5 to 9 (AdP, 2017). The cooling fluid is a mixture of ethylene glycol and water, with a concentration of 30% in volume of ethylene glycol. In some experiments water was mixed with THF as a way of shifting the temperature and pressure conditions required for hydrate continuous production, as well as reducing the heat of hydration.

3.2 Experimental Unit

The experimental system used in this work (see Figure 3.1) is called P01 and it is part of a project led by CoLAB NET4CO2 - Network for a Sustainable CO_2 Economy for continuous hydrate production.

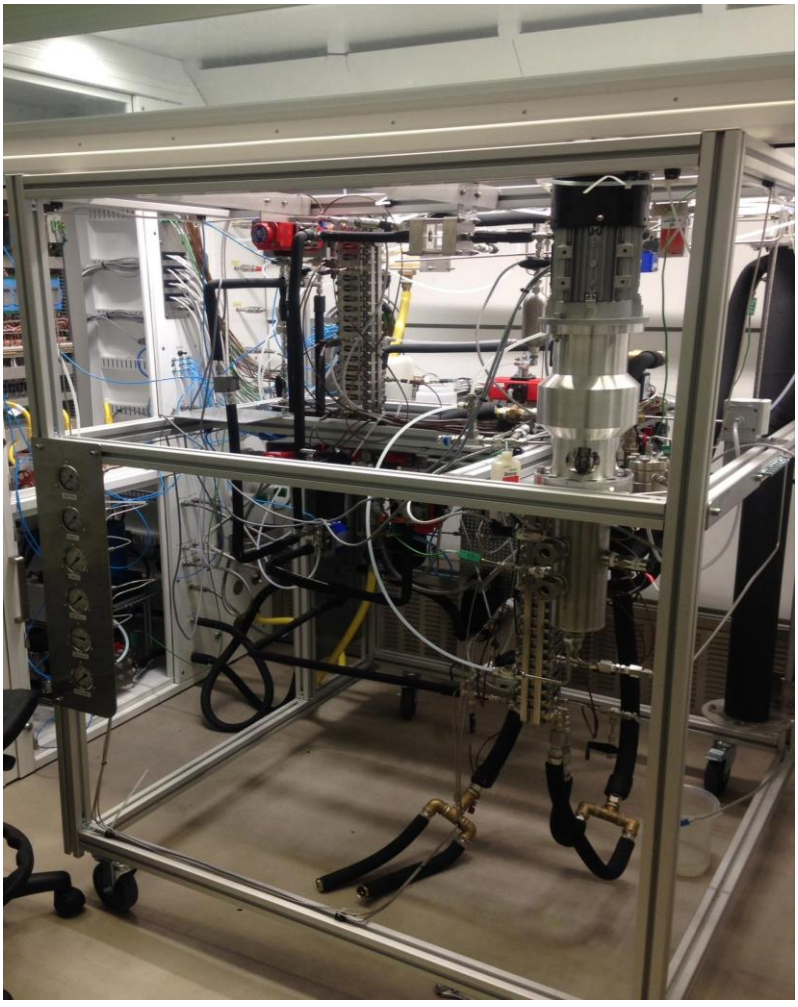

Figure 3.1: P01 experimental unit

Even though this unit is installed at the CoLab facilities, it is placed inside a walk-in fume hood, which guarantees safe operation conditions in case of gas leakage, and the electronic components that control the process variables and conditions are placed in a separate compartment to assure their integrity.

This unit allows simultaneous injection of liquid and gas to a NETmix unit as well as controlling the conditions needed to produce hydrates safely and successfully at CO_2 flow rates ranging from 0,5 to 2 $kg \cdot h^{-1}$, and H_2O flow rates ranging from 5 to 30 $kg \cdot h^{-1}$. It also allows the monitoring of several variables that allow the analysis of the system, making it possible to perform energy and mass balances to the NETmix units, providing more insight into the physical and thermodynamical conditions that make hydrate production viable.

3.3 Process Flow Diagram

The P01 is a complex unit with multiple features and applications. Its process flow diagram is presented in Figure 3.2 and a detailed description is provided below.

Water is fed to the system through a vessel (W-E-1) filled with fresh water controlled by an automated ball valve (W-V-1). The vessel is at atmospheric pressure and its temperature is monitored by a thermocouple (TT W-I-1). The filling of the vessel is controlled through two level transducers (LT W-I-2 and W-I-3), installed at different heights. These act on the valve W-V-1, opening the valve when the bottom-level transducer does not detect water, allowing the filling of the tank, and closing the valve once the top-level transducer detects water. There is a third float level transducer (LT W-I-4) that prevents the pump from being damaged in case of water scarcity.

A diaphragm pump (W-E-2) pumps water into a plate heat exchanger (W-E-7) where its temperature is controlled by means of a cooling fluid flowing in counter current. Upstream this heat exchanger, a check-valve (W-V-3) is installed to avoid any backflow, and the valve (W-V-4) placed immediately afterwards allows to prime the pump or purge of any undesired flows in the system. An inline filter (W-E-6) is installed in the water line, to prevent the entry of solid impurities in the system. Water flow rate is measured using a Coriolis flow meter (W-M-1). Downstream the exchanger W-E-7, the temperature and pressure are monitored using a thermocouple (TT W-I-6), pressure transducers and pressure gauges (PT W-I-7 and PG W-I-8), prior to entering the NETmix unit (H-E-1). A check-valve (W-V-6) is installed upstream the first NETmix (H-E-1), once again to prevent backflow.

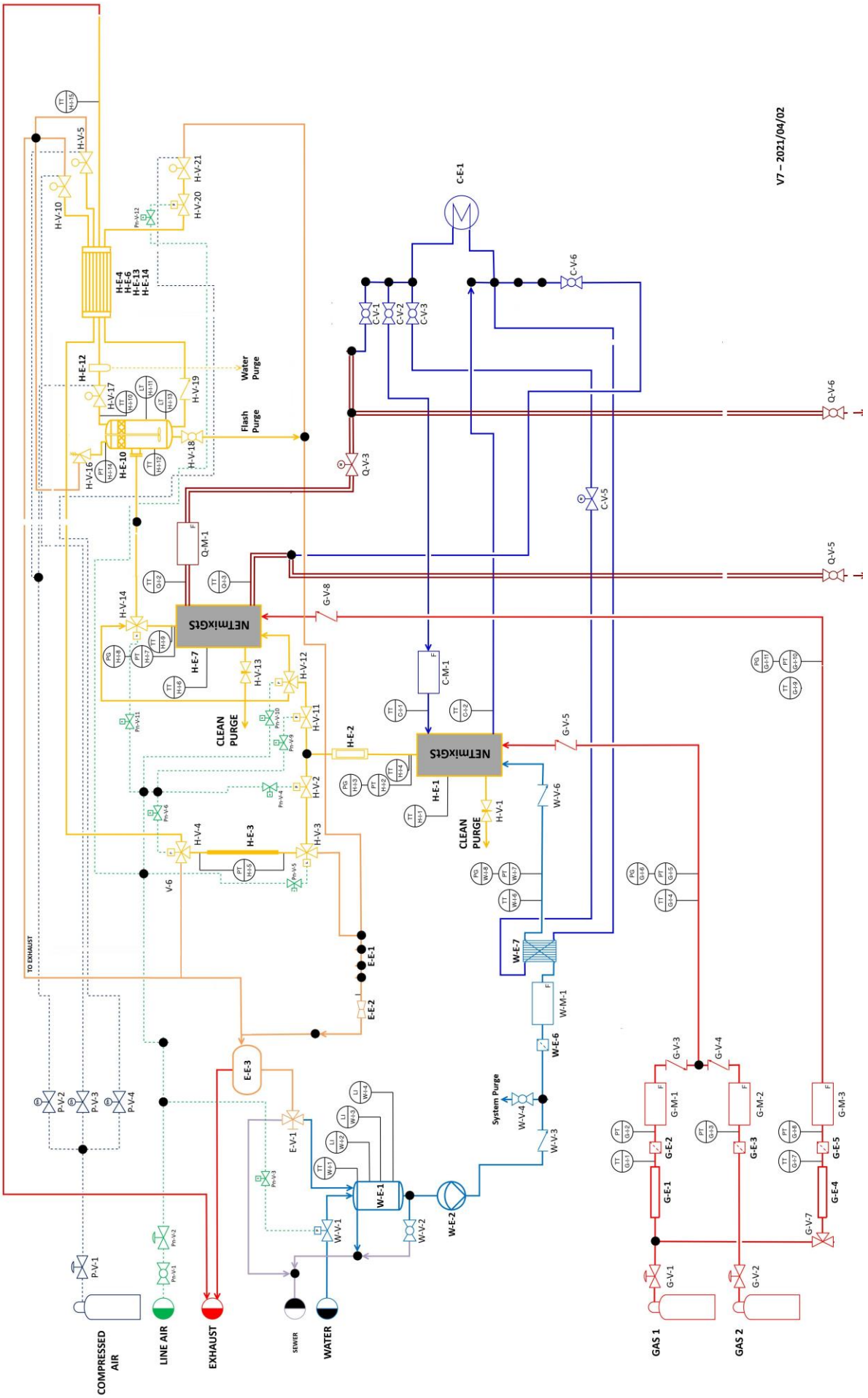

Figure 3.2: P01 process flow diagram. (NET4CO2, 2021)

Carbon dioxide and nitrogen are contained in pressure vessels and can be fed to the system through lines gas 1 and gas 2, respectively. The setup also allows the feeding of a mixture of N_2/CO_2 that replicates the desired flue gas, although N_2 has not been used for the work produced in this thesis. The unit is designed so that customized gas mixtures can be fed, by independently setting the flowrate of each gaseous component that constitutes the mixture. The pressurized cylinders contain pressure reducers (G-V-1 and G-V-2) and the gas flows through a line setup with inline filters (G-E-2, G-E-3 and G-E-5) followed by mass flow controllers (G-M-1, G-M-2 and G-M-3). There are check-valves (G-V-3 and G-V-4) installed downstream these MFC's, to prevent cross-contamination of the controllers, as well as upstream the NETmix unit (H-E-1), immediately after the thermocouple (TT G-I-4), pressure transducers and pressure gauges (PT G-I-5 and PG W-I-6), which monitor and assure the desired conditions to the process. A three-way valve (G-V-7) is set up so that CO_2 can be fed solely to a second NETmix unit (H-E-7).

In the NETmix unit (H-E-1), both water and carbon dioxide meet each other. Simultaneously, cooling fluid is fed to the NETmix cooling plates to remove heat released during gas dissolution and hydrate formation. The cooling fluid is an aqueous mixture with 30% glycol which has its flow rate regulated by a ball valve (C-V-2) and measured through a ultrasonic flow meter (C-M-1), and it is in a closed loop between a central chiller (C-E-1) and the NETmix unit. The cooling fluid inlet and outlet temperatures are measured through thermocouples (TT C-I-1 and TT C-I-2). As it is important to perform the energy balances, monitor the hydrate slurry production and pressure drop in the NETmix, temperature and pressure are also measured at this unit outlet via thermocouples (TT H-I-4) and pressure transducers (PT H-I-2 and PG H-I-3).

The stream exiting the first NETmix enters a visualizing sampler window (H-E-2) and downstream, it can either flow to a vessel (H-E-3) for sample extraction or be routed to a second NETmix unit (H-E-7) through two pneumatically-actuated valves (H-V-2 and H-V-11). If the stream flows to the vessel its pressure is monitored by a pressure transducer (H-I-5), to control the conditions of the collected sample and prevent any damage to the unit, but, by means of a three-way valve (H-V-3), it can also be purged to exhaust or to a vessel (E-E-3) where the water is separated from the gas, and can either be recirculated to the water vessel (W-E-1) or go directly to the sewer. If the stream is routed to the second NETmix, the setup also allows it to bypass this second unit through means of two actuated three-way valves (H-V-12 and H-V-14). The second NETmix outlet stream is monitored by thermocouples (H-I-9) and pressure transducers (H-I-7 and H-I-8) to maintain safety to the unit and perform energy balances. Similar to the first unit, an electronically flow regulating valve (Q-V-3) controls the feed of cooling fluid to the NETmix and a flow meter (Q-M-1) measures the flow rate of this fluid, while thermocouples (TT Q-I-2 and TT Q-I-3) monitor the temperature of the inlet and outlet.

After exiting the second NETmix, or bypassing it, the stream reaches a flash tank (H-E-10). The pressure inside the tank is controlled through a back pressure regulator (BPR) installed downstream the vessel (H-V-5 and H-V-10). There is a relief valve (H-V-16) installed in the flash tank to ensure safe operation in case of pressure surge. Level transducers (H-I-11 and H-I-13) allows the control of the level of the liquid phase in the tank, and a ball valve (H-V-18) purges any excess. The temperature and pressure in the tank are measured through a thermocouple (H-I-12) and a pressure transducer (H-I-14).

Most valves described are automatically controlled using a pneumatic system. This system uses pressurized air which has a pressure reducer (Pn-V-1) to lower the pressure from the line to around 10 bar. This air line is then fed to valves actuated through solenoid actuators (Pn-V-3 to Pn-V-12). The setup also uses high-pressure compressed air which is needed to control the BPRs (H-V-10 and H-V-15) and pressurise the flash separator also through a BPR (H-V-17) at the start of the process. This system requires air with different pressures since the equilibrium pressure for hydrates can range from 15 to 30 bar.

An Optomotive Velociraptor high speed camera is placed facing the visualizing sampler window (H-E-2) to observe changes in the outlet NETmix flow not visible to the naked eye as well as record them.

Although not mentioned in this process flow diagram description, the unit presents many other features such as measurement of differential pressure to determine fluid viscosities and gas chromatography to analyse composition of outlet gases, among others. However, those features were explored but not tested in this work.

3.4 NETmix Units

Despite the fact that this work is a continuation on M.F.Costa PhD thesis, the biggest difference is the central piece of the unit, the NETmix. M.F. Costa's work in continuous production of hydrates used a microNETmix that presents different characteristics from the one used in this work which are shown in Table 3.1.

Table 3.1: microNETmix and P01 NETmix dimensions. Sources: [10,39]

Parameter	*Unit*		
		microNETmix	**P01 NETmix**
		Value	
Plate length	mm	140	73
Plate Height	mm	120	620
Plate thickness	mm	3	3
Chamber diameter	mm	3,3	3,4
Number of rows in NETmix plate	-	23	144
Number of columns in NETmix plate	-	7-8-7	8-9-8
Number of NETmix plates	-	3	1

The NETmix unit has three types of plates which can be observed in Figure 3.3:

• A NETmix plate, where the networks of chambers and channels are machined, and which go inside the reactor. Streams of CO_2 and water will continuously flow in these plates to form hydrates.

• Two thermal plates made of an array of machined fins, which improve the transfer of heat produced from the production of hydrates. The coolant will circulate in this plate, which can be in counter flow or parallel flow to NETmix plate flow direction.

• Two closing plates, where the hydraulic connections will be connected, and through which the sealing is done by the mechanical action of screws, to contain the internal pressures in the NETmix plate of about 30 bar.

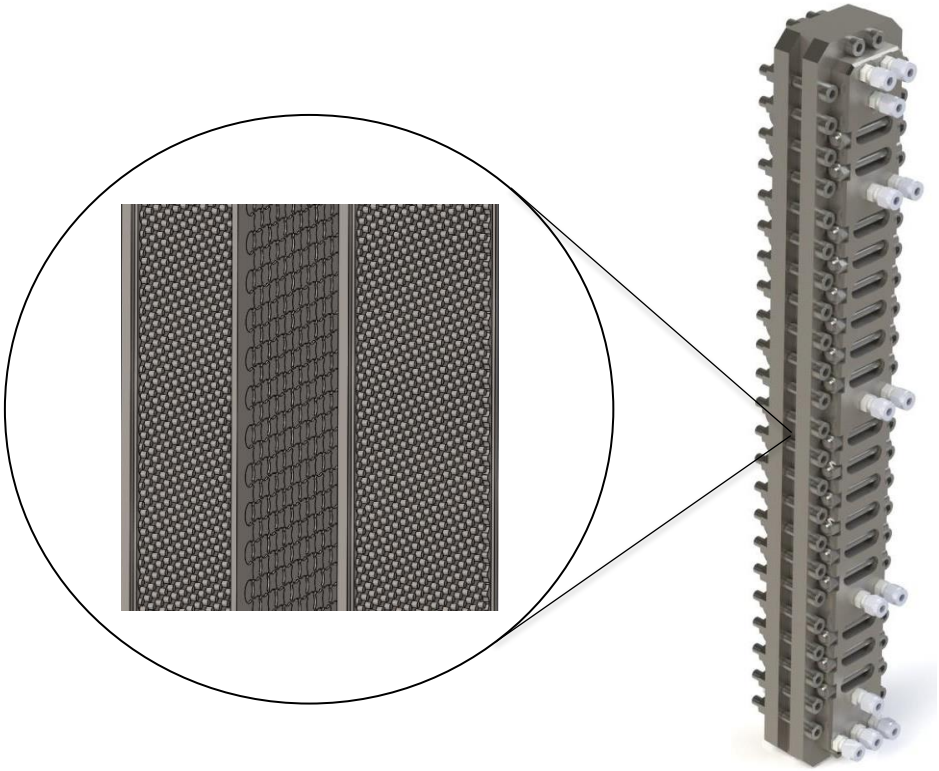

Figure 3.3: P01 NETmix reactor with cooling plates and network plate detail. Source: [39]

3.5 Experimental Procedure

The described unit was tested to study and measure some of its major assets for implementation, either in research and development or desired industrial projects, from superior heat removal and mixing capability to a solution for carbon capture.

3.5.1 Heat Transfer Performance

Continuous production of hydrates requires the removal of the heat released during both gas dissolution in water and hydrate crystallization. For that matter it is very important to determine if the NETmix heat transfer coefficient allows high amounts of heat to be completely removed during a continuous process. Previous studies on the convective heat coefficient had already been conducted, so only the effect of the increasing of the water flow rate on the overall heat coefficient was studied throughout this work.

The NETmix was carefully insulated so that the amount of heat lost to the surroundings can be negligible, and heat transfer would only occur between the cooling fluid and the water flowing through the NETmix network plates. An external heater was added to the system using the same thermal fluid which was fed to the plate heat exchanger to heat the temperature of the feeding water up to 40ºC, while the cooling fluid, fed to the NETmix, was cooled by the central chiller to a temperature of -2ºC.

The thermocouples at the inlet and outlet of the NETmix were thoroughly calibrated using a single point with ice in water, to assure integrity of the data collected.

This procedure was replicated in both NETmix units to evaluate both the quality of the isolation and validate the heat transfer performance of the equipment.

3.5.2 Mass Transfer Performance

To determine the capacity of the NETmix to promote dissolution of gas in liquid, both CO_2 and water were injected simultaneously to the unit. Studies with N_2 were not carried out since the installed mass flow controllers did not have enough resolution to allow this test to be preformed.

Since solubility increases with temperature and pressure, both these parameters were shifted in a large range slightly above hydrate formation conditions. Mass transfer coefficient is not only controlled by the diffusion but also by the contact of phases which is increased by the mixing intensity, meaning that both liquid and gas flow rate are an important factor to gas dissolution.

Therefore, a set of conditions (temperature, pressure, and water flow rate) were kept constant for each run, while the gas flow rate was carefully increased. A high-resolution and high-speed camera was placed in front of the visualiser downstream the NETmix, so as to capture the exact moment and flow rate at which the unit was unable to totally dissolve the CO_2 on the water.

Since this method had to be carried out slowly and carefully to assure its validation, the small value of the gas flow rates required the mass flow controllers to be calibrated for each single experiment.

The experiments were performed at conditions slightly above the hydrate formation so that no external factors, like hydrate nucleation, would affect the obtained results.

3.5.3 CO2 Hydrate Production

Hydrate production requires simultaneous injection of CO_2 and water as well as favourable conditions of temperature and pressure. Nonetheless, heat removal is detrimental to meet those conditions, as well as good mixing, which will meet the gas saturation levels that allows hydrate formation.

A wide range of values for each variable of the continuous hydrate production were determined and each run was performed for 30 minutes to assure steady state stability as well as to certify the viability of long periods of hydrate production. In some of the runs, THF was added to the water as a hydrate promoter, which allow gas hydrates to be produced at conditions that made the continuous production smoother, such as higher temperatures, lower pressure, and hydration heat.

3.5.4 Gravimetry Analysis

Following the production of CO_2 hydrate, for each pressure where hydrates were successfully produced, a sample was extracted to determine the amount of gas in the sample collected. The sample was stored in a freezer in a previously weighted and insulated container where it stabilized and achieved a metastable state. In this state there is still residual gas release, so the analysis was carried out as soon as it could possibly be.

After stabilizing, the container was carefully carried, to minimize the heat exchange, and placed on a scale where the guest molecules slowly gasifies, reducing its weight. A point was registered every 2 minutes to monitor the gas release rate.

4 Heat transfer performance

The purpose of this set of experiments was to study the capacity of NETmix to remove heat from the system, which is of great importance for the production of hydrates and adjacent hydration heat released upon formation.

4.1 Introduction

4.1.1 Heat transfer

Heat transfer in this system occurs through two mechanisms: conduction and convection.

Conduction is the transfer of heat from one part of a body to another part of the same body without significant displacement of its particles. This phenomenon was first described in a form of an equation by Fourier in 1822[41], which for a plane wall can be written as:

$$\dot{Q} = kA\,\frac{T_1 - T_2}{x} \tag{3.1}$$

Where $\dot{Q}$ is the heat transfer rate, in W; A is the area normal to the direction of the heat flow, in m^2; $T_1 - T_2$ is the difference in temperature between the two points studied in the transfer of heat, in ^oC; x is the thickness of the solid in the direction of the heat flow, in m; and k is the material's thermal conductivity, in $W{\cdot}m^{-1}{\cdot}{}^oC^{-1}$.

Heat transfer due to convection involves the energy exchange between a surface and an adjacent fluid. Even when a fluid is flowing in a turbulent manner past a surface, there is still a layer, sometimes extremely thin, close to the surface where flow is laminar; also, the fluid particles next to the solid boundary are at rest[42]. These particles form a "film" where the flow which is essentially in laminar motion and through which heat is transferred by molecular conduction[41].

The rate equation for convective heat transfer was first expressed by Newton in 1701, and is referred to as the Newton rate equation or Newton's ''law'' of cooling:

$$\dot{Q} = hA(T_2 - T_1) \tag{3.2}$$

Where $\dot{Q}$ is the heat transfer rate, in W; A is the contact area normal to the direction of the heat flow, in m^2; $T_2 - T_1$ is the difference in temperature between the fluid and the surface of the material, in ^oC; and h is the convective heat transfer coefficient, in $W{\cdot}m^{-2}{\cdot}{}^oC^{-1}$.

Rewriting both Equations 3.1 and 3.2 in terms of $(T_2 - T_1)/\dot{Q}$, we get what can be described as the resistance of the mechanism to heat transfer:

$$R_{cond} = \frac{T_2 - T_1}{\dot{Q}} = \frac{x}{kA} \tag{3.3}$$

$$R_{conv} = \frac{T_2 - T_1}{\dot{Q}} = \frac{1}{hA} \tag{3.4}$$

The higher the resistance, the more difficult it is for the medium to transport heat. In a case where the removal of heat has an important impact, low heat transfer resistance is desired.

Resistance by conduction in solids can only be altered by either changing the material or by changing the thickness of the solid in the direction of the heat flow. In convective resistance, on the other hand, the resistance of the film to heat flow depends not only on the fluid, but also on the system hydrodynamic conditions[42].

4.1.2 Overall heat transfer coefficient

For systems involving combination of mechanisms, one can write the heat transfer rate as an association of all these resistances found in the system. The global heat transfer coefficient in the direction normal to the NETmix plate flow direction can be determined by the association in series of the resistances of both NETmix ($\frac{1}{h_{\text{NETmix}}}$) and cooling plates ($\frac{1}{h_{\text{coolant}}}$), at the liquid level through convection, and of the solid that separates both plates ($\frac{x_{\text{plate}}}{k_{\text{plate}}}$), through conduction[10]. Assuming equal area for heat transfer in each resistance, the global heat transfer coefficient can be determined from:

$$U = \left(\frac{1}{h_{\text{NETmix}}} + \frac{x_{\text{plate}}}{k_{\text{plate}}} + \frac{1}{h_{\text{coolant}}} \right)^{-1} \tag{3.5}$$

Where *U* has units of $W \cdot m^{-2} \cdot {}^{o}C^{-1}$. A comparison between those terms allows one to understand importance of each of the thermal resistances of the system, and optimize the system either for minimizing or maximizing heat transfer.

In a device such as NETmix, where heat is removed from a fluid, the amount of heat can be determined by the following equation:

$$\dot{Q} = \dot{m} \cdot c_p \cdot (T_{inlet} - T_{oulet}) \tag{3.6}$$

Where $\dot{m}$ is the water fluid flow rate, in $kg \cdot h^{-1}$; c_p is the fluid specific heat, in $J \cdot kg^{-1} \cdot {}^{o}C^{-1}$; and the temperatures are those obtained at the inlet and outlet of the system in study, in ^{o}C. This can be useful to determine the overall heat coefficient since the amount of heat removed from the fluid is the same amount transferred between water and coolant:

$$\dot{Q} = \dot{m} \cdot c_p \cdot (T_{inlet} - T_{oulet}) = U \cdot A \cdot \Delta T_{lm} \tag{3.7}$$

Where, for countercurrent flow ΔT_{lm}, in ºC, is

$$\Delta T_{lm} = \frac{(T_{NETmix,in} - T_{coolant,in}) - (T_{NETmix,out} - T_{coolant,out})}{\ln\left(\frac{T_{NETmix,in} - T_{coolant,in}}{T_{NETmix,out} - T_{coolant,out}}\right)} \quad (3.8)$$

In Equation 3.8, $T_{NETmix,in}$ and $T_{NETmix,out}$ are considered as the inlet and outlet temperatures of the system and are obtained from the bottom and top of the reactor, respectively. $T_{coolant,in}$ and $T_{coolant,out}$ are the temperatures of the cooling fluid at the top and bottom of the reactor, respectively, as both fluids exchenge heat while flowing in contercurrent to eachother.

4.2 Results

In this work, the same conditions presented in table 4.1 were replicated in both NETmix reactors.

Table 4.1: Conditions for heat transfer perfomance experiments

Fluid	*Inlet Temperature / ºC*	*Q / kg · h^{-1}*
Water	40	4 - 32 [1]
Coolant [2]	-1,5	533

1 Water flow rate was increased 2 kg/h for each run. Some points were omitted due to difficulties in performing the experiment.

2 Due to the central chiller dimensions the inlet temperature determined for the coolant might suffer fluctuations.

The data collected from the experiment's water and coolant temperatures are plotted below in Figures 4.1 and 4.2, as well as the water flow rate shifts during each experiment.

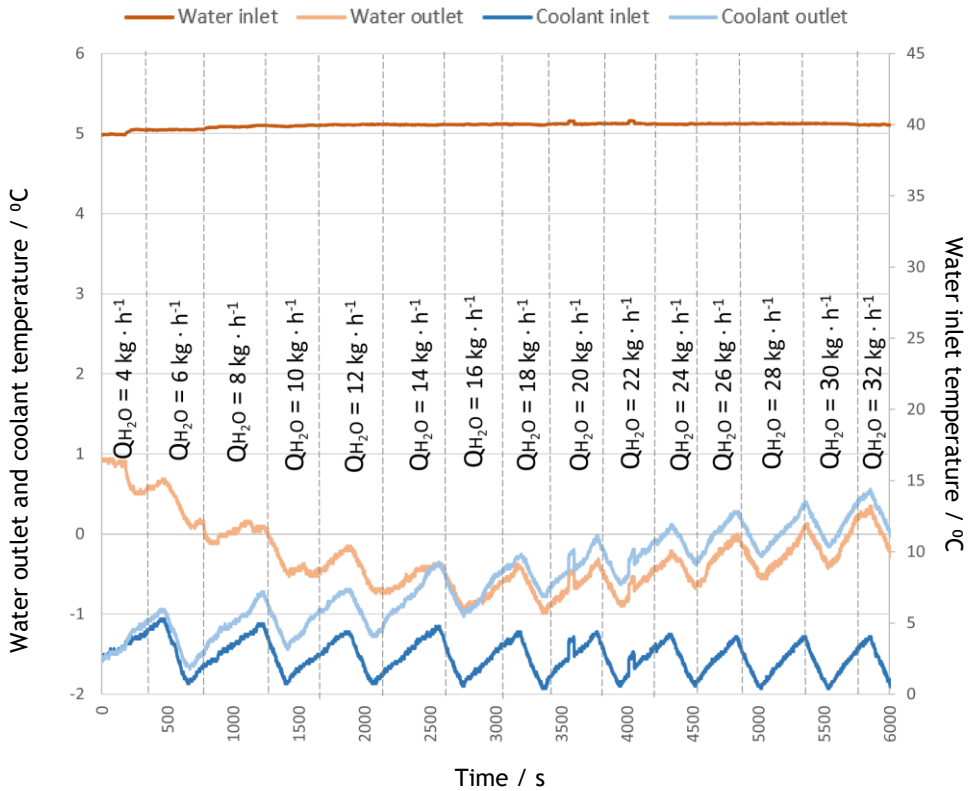

Figure 4.1: Data collected from NETmix H-E-1 temperatures during experiment

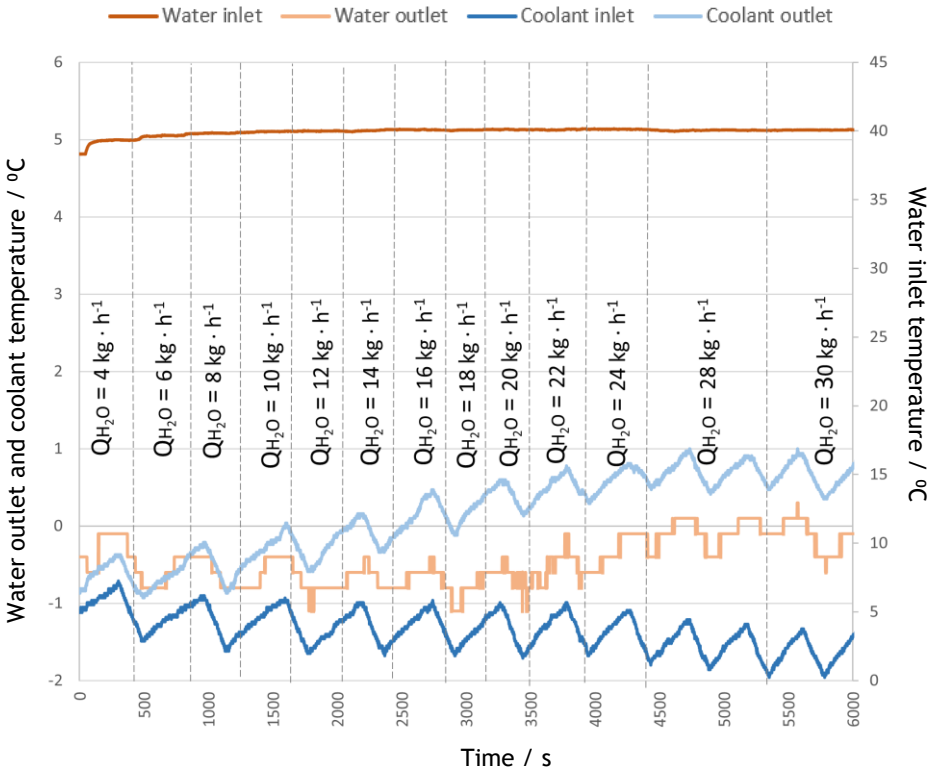

Figure 4.2: Data collected from NETmix H-E-7 temperatures during experiment

The heat exchanged in the system is estimated by performing an enthalpy balance to the water, instead of the cooling fluid. This justified by the fact that the water flowrate is lower than the flowrate of the cooling fluid, and consequently, the temperature decrease is higher than the temperature increase in the cooling fluid, and thus reducing the error associated to the measurements. Moreover, the coolant is subject to oscillations during the runs, as the result of the internal control algorithm of the chilling unit.

From this data and Equation 3.6, it is possible to estimate the overall heat transfer coefficient. This coefficient, as well as the respective resistance, as a function of the water flow rate for both NETmix units, are plotted in Figure 4.3:

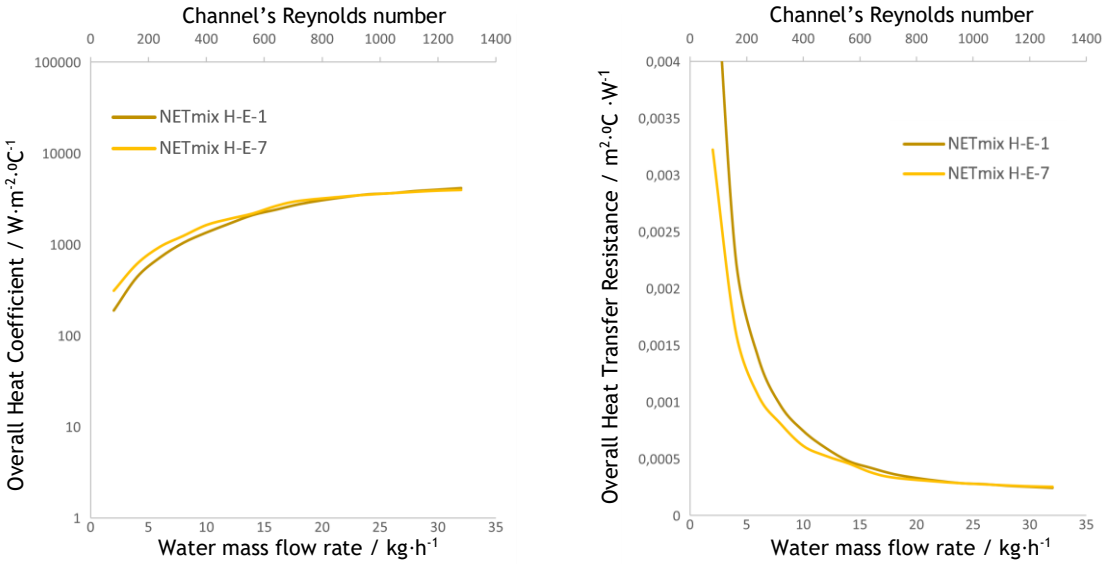

Figure 4.3: Left: Calculated overall heat transfer coefficient vs water mass flow; Right: Overall heat transfer resistance vs water mass flow

Figure 4.3 shows that the overall heat transfer coefficients for both NETmix units are in agreement with each other ranging from 200 $W \cdot m^{-2} \cdot {}^{o}C^{-1}$ for a channel's Reynolds number of 80 to 4000 $W \cdot m^{-2} \cdot {}^{o}C^{-1}$ for a channel's Reynolds number of 1250. Even though the increase in the coefficient was higher after the flow in the reactor surpassed its Reynolds channel's critical number, its growth was fairly constant during the entire experiment.

Since the structural characteristics of the NETmix network plates are known as well the convective coefficient from the coolant side (Appendix A), it was possible to determine the convective heat transfer coefficient from the NETmix side from equation 3.4. Since all resistances are now known, it is possible to study the weight of each one in the overall heat transfer resistance. The percentage each resistance has in the heat transfer mechanism of the NETmix is plotted below in Figure 4.4 as function of the water mass flow rate:

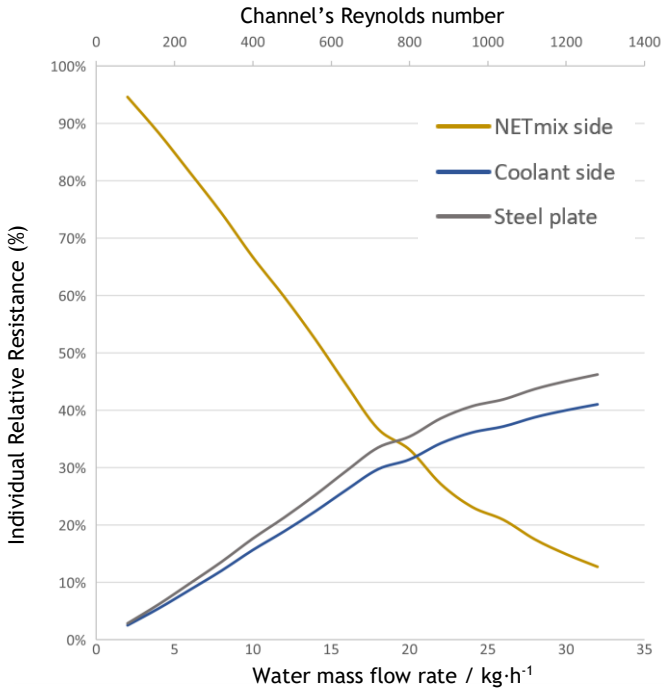

Figure 4.4: Relative resistance for each NETmix resistance vs water flow rate

The flow rate of the coolant is already maximized and there is no possibility of changing the material or the dimensions of the NETmix network plate, thus, the best way to increase heat transfer rate is by working at a Reynolds higher than 800, in which the resistance of the NETmix plate is similar to the other resistances in the system and, from this point on, the main limitations to heat transfer become the convection in the coolant side and conduction through the plate.

Moreover, being that not only temperature but also pressure are measured both at the outlet and inlet of the NETmix, it is possible to compare the pressure drop in the unit to its theoretical

value with the mechanistic model proposed by Fonte et al. (2013). Both pressure data collected and the theoretical model are presented in Figure 4.5.

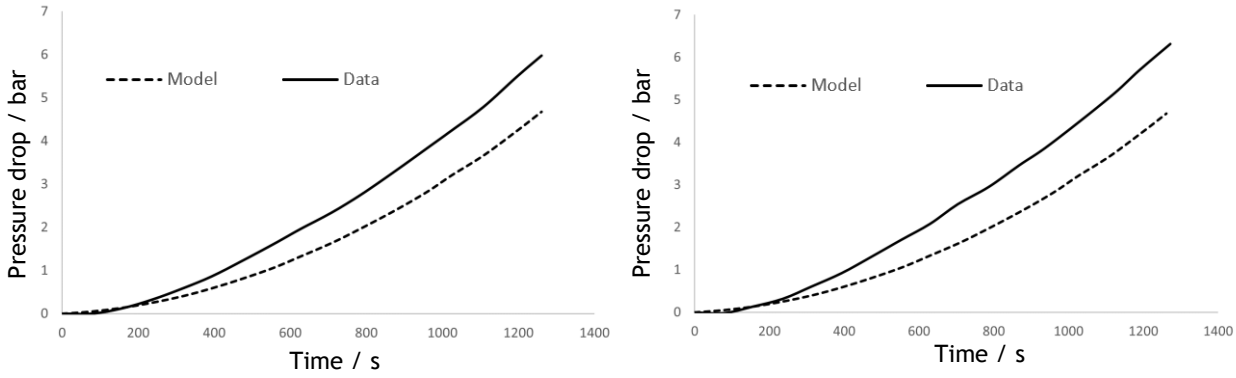

Figure 4.5: Pressure drop for NETmix H-E-1 (left) and H-E-7 (right)

The main reason why the data value differs from the theoretical model is that this equation only considers the pressure drop in the network and the system tested has check-valves before the NETmix reactors as well as gas injectors and manifolds which are not considered in the mode. For NETmix H-E-7 the pressure drop from the data seems to be slightly higher then the NETmix H-E-1 value which could be explained by the longer path the fluid has to travel to reach the reactor. The model also has its basis on the fluid traveling along the shortest path (see Figure 4.6), which is hard to achieve as the reactor is too complex to be physically possible for all fluid molecules to take this same path.

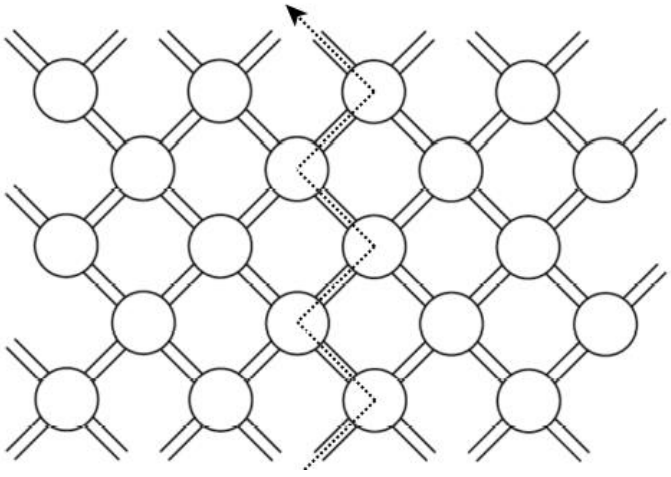

Figure 4.6: Shortest path for traveling fluid along NETmi network. (Fonte, 2013)

5 Mass Transfer Performance

The objective of this study is to determine whether the NETmix reactor has higher mass transfer coefficients than other absorption devices available, many of them already implemented in an industrial environment. This is of major importance for a process such as continuous production of gas hydrates since supersaturation of the medium is detrimental for its formation.

5.1 Mass Transfer Between Phases

When material is transferred from one phase to another across an interface that separates the two, the resistance to mass transfer in each phase causes a concentration gradient in each side of the interface, a theory initially suggested by Whitman to explain this process[43]. Figure 5.1 provides a visual representation of the mass transfer system and respective resistances.

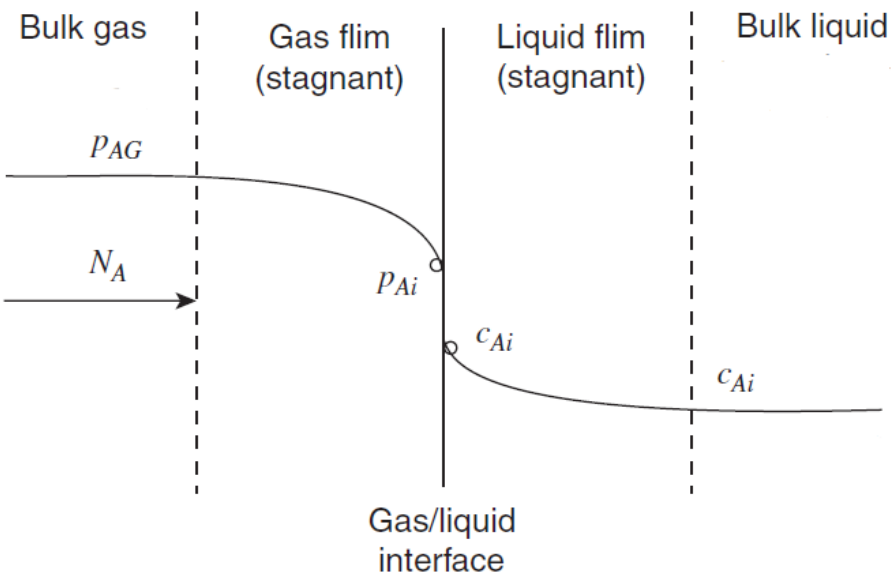

Figure 5.1: Concentration gradients between two contacting phases where solute is transferred from gas to liquid.

The concentrations of the solute in both phases adjacent to the interface are generally unequal but usually are assumed to be related to each other by the laws of thermodynamic equilibrium such as Henry's law, for dilute solutions (Equation 5.1). Thus, it is assumed that the thermodynamic equilibrium is reached at the gas-liquid interface almost immediately when a gas and a liquid are brought into contact[41].

$$C_g^i = \mathrm{H} \cdot C_L^i \tag{5.1}$$

For systems in which the solute concentrations in the gas and liquid phases are low, i.e., in dilute systems, the rate of transfer may be expressed by equations that predict that the rate of mass transfer is proportional to the difference between the bulk concentration and the concentration at the gas-liquid interface.

In many gas–liquid processes, the gas is sparged into a unit together with liquid that is mixed by mechanical stirring. The unit promotes gas–liquid contact by breaking up the gas bubbles and dispersing them throughout the liquid volume. A similar process can be conceptualized in the NETmix when water and CO_2 are simultaneously injected, as a result of the chaotic and oscillatory flow regime that can be observed. Due to the continuous collision of the gas bubbles, the interfacial area for mass transfer is impossible to measure. Consequently, measured mass-transfer coefficient for these units is reported as a capacity coefficient[41] or volumetric mass transfer coefficient[42] $K_L a$.

$$N_{CO_2} = K_L a \cdot (C_L^* - C_L) \tag{5.2}$$

Where N_{CO_2} is the dissolution rate in mol·m^{-3}·s^{-1}, C_L is the concentration in liquid and C_L^* is the concentration in liquid in equilibrium with the gas, both in mol·m^{-3}, and the mass-transfer coefficient, K_L *or* K_G *in* m·s^{-1}, is lumped together with the parameter a, which is defined as

$$a = \frac{A_i}{V} = \frac{area\ valiable\ for\ interphase\ mass\ transfer\ (\mathrm{m}^2)}{liquid\ volume\ (\mathrm{m}^3)} \tag{5.3}$$

5.2 Results

At the beginning of each run, the valve that controls the CO_2 flow rate is completely closed. The flow rate is then gradually and slowly increased, so that steady state is reached, using increase steps as small as allowable by the mass-flow controller, which is 0,01 kg·h^{-1}. The flow rate is increased until bubbles are visible in the visualizing sampler window, thus indicating that CO_2 can no longer be absorbed by the water. Both situation of complete absorption and saturations are evidenced in Figure 5.2a and 5.2b, respectively.

Since the main goal of the unit is to continuously produce hydrates, it is important to understand whether supersaturation might be achieved and, for that reason, all experiments (see Table 5.1) were performed at 5 ºC as an indicative value close to the conditions that will be needed later for the NETmix to be able to form hydrates.

Table 5.1: Conditions for mass transfer perfomance experiments

Experiment	*Relative Pressure*[1] / bar	*Water flow rate* / kg·h^{-1}
E – 1	5 - 30	10
E – 2	5 - 30	12,5
E – 3	5 - 30	15
E – 4	5 - 30	17,5
E – 5	5 - 30	20
E - 6	5 - 30	25

1 for each run of every experiment the pressure in the system was increased by 5 bar

After determining the maximum CO_2 flow rate for which gas is absorbed by the liquid phase, the concentration of gas in the liquid can be calculated and, assuming constant pressure and temperature inside the reactor and assuming that the concentration of CO_2 in water at the inlet is zero, the volumetric mass transfer coefficient is estimated performing a mass balance in the NETmix:

$$Q_{\mathrm{H_2O}} \frac{dC_L}{dV} = K_L a \cdot (C_L^* - C_L) \quad <=> \tag{5.4}$$

$$<=> \quad K_L a = \frac{Q_{\mathrm{H_2O}}}{V_{\mathrm{NETmix}}} \cdot \ln\left(\frac{C_L^*}{C_L^* - C_L}\right)$$

Where V_{NETmix} is the NETmix network internal volume, which is 6,3 cm^3.

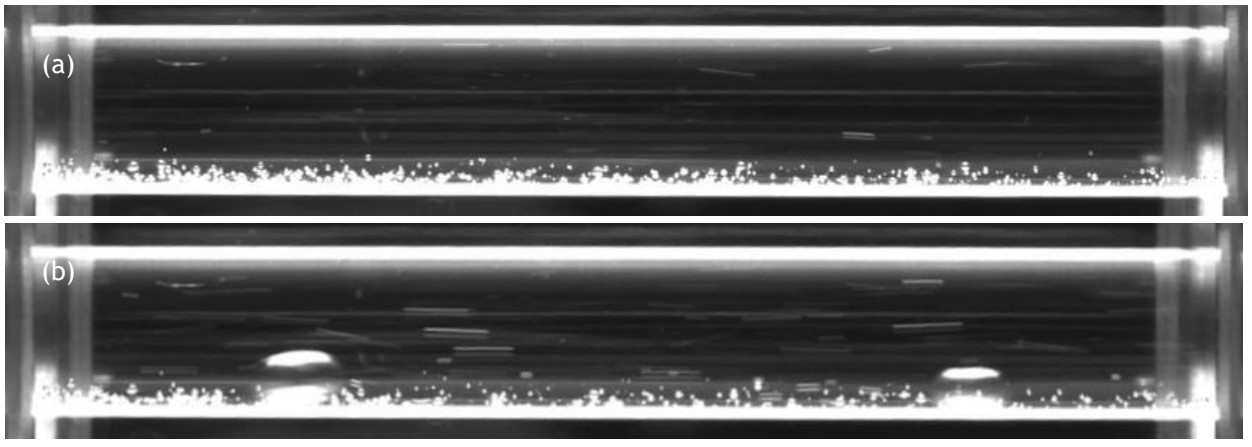

Figure 5.2: Two observed cases for mass transfer experiments: (a) complete absorption and (b) water saturation

The data obtained from applying equation 5.4 to the obtained values in the experiments is plotted in Figure 5.3 as a function of the relative pressure in the NETmix:

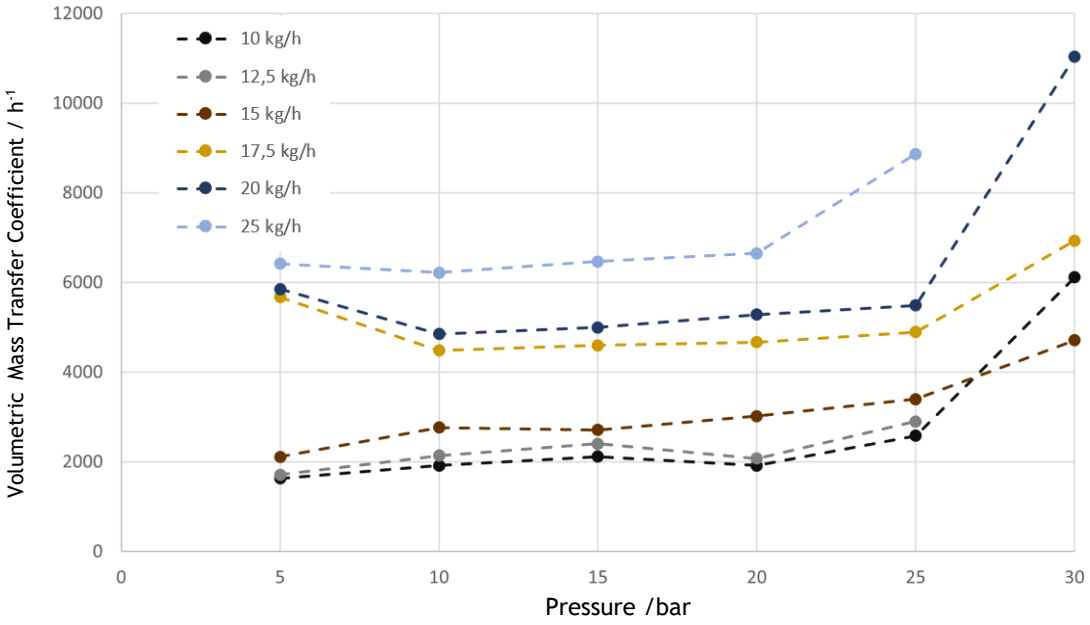

Figure 5.3: Liquid-side volumetric mass transfer coefficient for each water flow rate by the NETmix relative pressure

The NETmix could achieve volumetric mass transfer coefficient ranging from about 2000 h^{-1} for a Reynolds channel number of 264 to about 6200 h^{-1} for a Reynolds channel number of 661, which is considerably higher than other absorption equipment's that can typically only reach coefficients as high as 3500 h^{-1} [43] (see Figure 5.4).

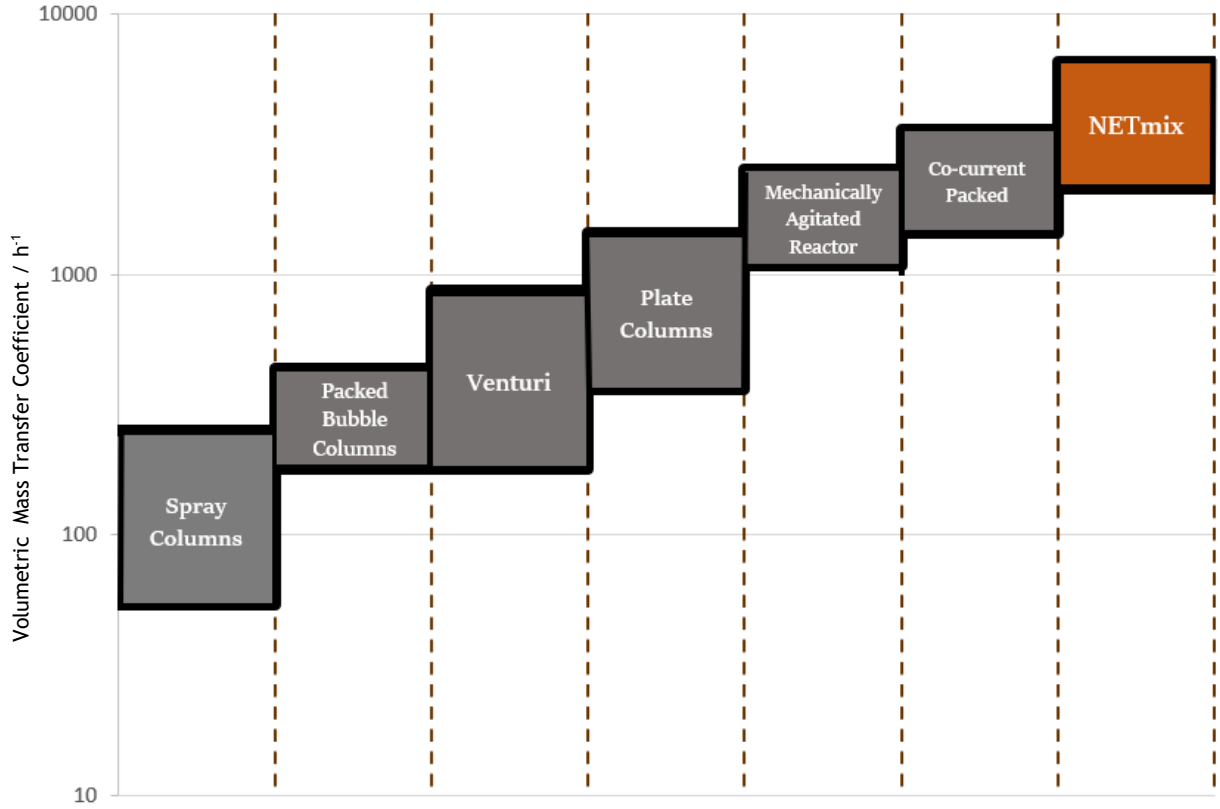

Figure 5.4: Volumetric mass transfer coefficient comparison between typical absorption equipment devices and NETmix.

The increase in volumetric mass transfer coefficient does not seem to be directly affected by the water flow rate, apart from the constant increase the higher the flow rate is. Nonetheless, a bigger difference can be observed for flow rates higher than 15 $kg \cdot h^{-1}$, where the mass transfer resistance seems to suffer a substantial decrease.

Another phenomenon observed in the data is the high increase in CO_2 consumption for pressures of 25 bar and above which translates in an exponential increase in the capacity coefficient. The reason for this might be that as the conditions for hydrate formation are approached, the induction of nucleation might interfere with the system consuming more gas to achieve supersaturation[24] (Figure 5.5).

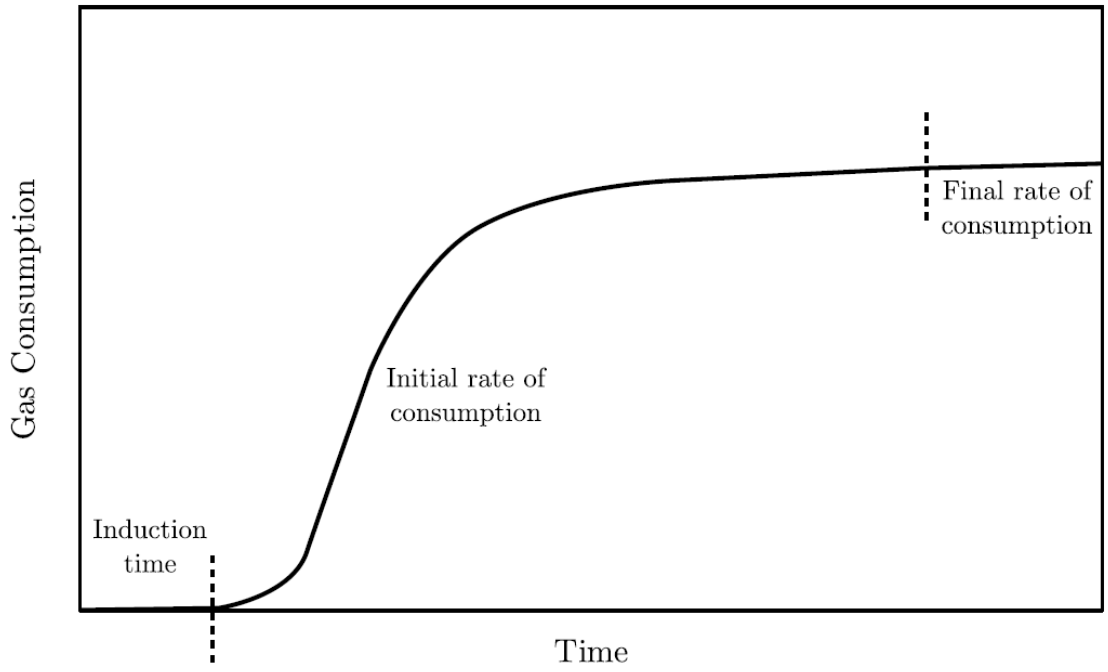

Figure 5.5: Gas consumption vs time for hydrate formation. (Sloan, 2007)

6 Continuous CO_2 Hydrate Production

Once it has been proved the NETmix capabilities to both exchange heat and enhance gas-liquid mass transfer, the following step is to assess the capacity of the technology to continuously produce CO_2 hydrates. The main goal of this study is to check whether hydrate is formed or not, and to monitor the unit's variables to ensure the stability of the process.

6.1 Continuous CO_2 Hydrate Production

Taking into account the thermodynamic conditions at which hydrates can be formed, that are already known, a set of runs was prepared. Also, with the data gathered in the dissolution experiment results from Chapter 5, it was possible to design this experiment with confidence that gas would be completely absorbed by water since supersaturation must be reached for hydrate to fully form.

The operating conditions for the experiments are presented in Table 6.1.

Table 6.1: Conditions for continuous CO_2 hydrate production experiments

Run	*Pressure* / bar	*Temperature* / ºC	*Water flow rate* / kg·h^{-1}	*CO2 flow rate* / kg·h^{-1}
R-1	20	1 - 2	10	0,5
R-2	20	0,6 - 1,8	10	0,75
R-3	20	0,2 - 1,2	10	1
R-4	20	0,2 - 1	10	1,25
R-5	20	1 - 3	10	2
R-6	20	1,2 - 2.2	20	0,5
R-7	20	1 - 2	20	0,75
R-8	20	1 - 2	20	1
R-9	20	0,8 - 1,2	20	1,25
R-10	20	0,4 - 1,2	20	1,5
R-11	20	0,8 - 1,2	20	2

Run	*Pressure* / bar	*Temperature* / ºC	*Water flow rate* / kg·h^{-1}	*CO2 flow rate* / kg·h^{-1}
R-12	30	2 - 4	10	0,5
R-13	30	1,5 - 3	10	0,75
R-14	30	1,5 - 2,5	10	1
R-15	30	1 -2	10	1,25
R-16	30	0,8 - 1,4	10	1,5
R-17	30	1,5 - 2,5	10	2
R-18	30	1 - 2,5	20	0,5
R-19	30	1 - 3,5	20	0,75
R-20	30	1,5 - 2,5	20	1
R-21	30	1,5 - 2,2	20	1,25
R-22	30	1,5 - 2	20	1,5
R-23	30	1,5 - 2	20	2

Regarding continuous production of hydrates, runs R-1 to R-5 were done to study the impact of CO2 flow rate, R-6 to R-11 were carried out to evaluate the impact of changing water flow rate and R-12 to R-23 were performed to study the impact of increasing pressure for all previous runs.

The runs able to successfully form hydrates were R-4, R-20, R-21, R-22 and R-23. Although these results do not provide a clear overview on the effect of shifting water or CO2 flow rate, hydrates formation seems to be easier for higher pressure. This should be expected since pressure increase represents an increase in the driving force.

The telemetry for the runs R-10 and R-22 represented in Figures 6.1 and 6.2, while others can be consulted in Appendix B.1. These were chosen as representative of a case where hydrates are formed or not, at different pressures, for the same water and CO2 flow rates and similar temperatures.

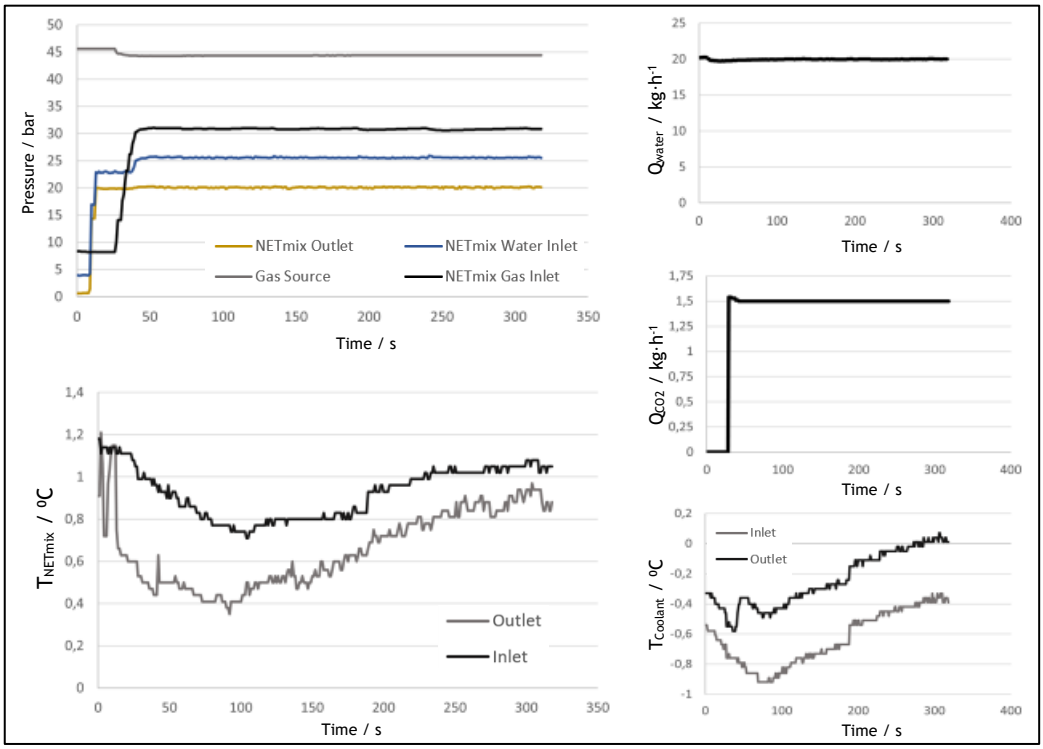

Figure 6.1: Telemetry from run R-10

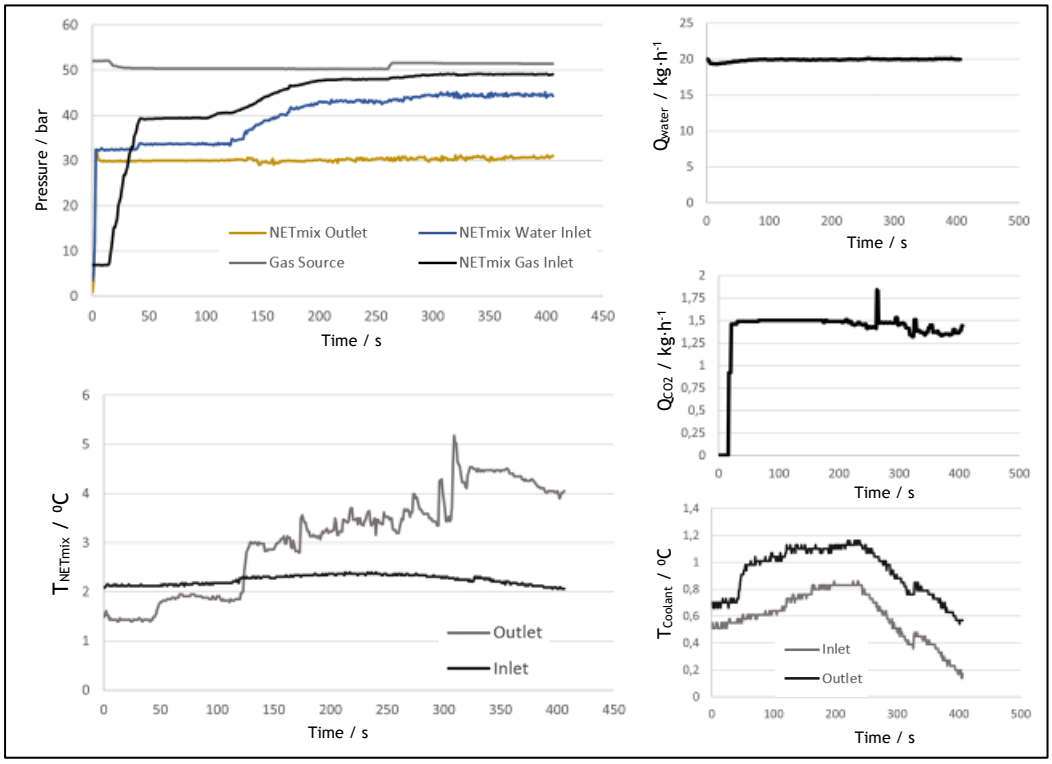

Figure 6.2: Telemetry from run R-22

Analysing both telemetries, both water and CO_2 flow rate were kept constant at all times, although the gas suffered a slight decrease when hydrates were formed. This is due to the fact that the mass flow controller needs to have a 8 bar pressure difference between the source and the NETmix inlet to guarantee the desired flow rate is reached.

The fluctuations in temperature of the cooling fluid fed to the NETmix unit, both at the inlet and outlet, are due to the control algorithm of the central chiller, in which the temperature is controlled within a band around the setpoint, creating the fluctuations observed.

One may question whether ice is being formed, instead of hydrates. However, since the temperature is always above 0 ºC, and the formation of the solid is only observed when the gas is introduced, it is known that hydrates, and not ice, are being produced.

The pressure drop in NETmix during both runs are presented in Figure 6.3.

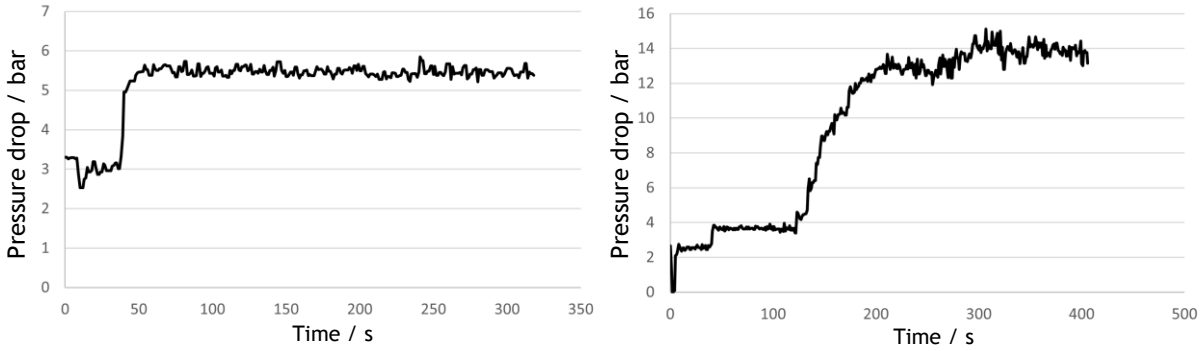

Figure 6.3: Pressure drop in the NETmix for R-10 (left) and R-22 (right)

The major differences between the experiments represented in Figure 6.1 and Figure 6.2 is that when there is formation of hydrates, the temperature at the NETmix outlet stream increases and so does the pressure at water and gas inlet. This shift on outlet temperature inside the NETmix is due to the heat of hydration released upon hydrate formation. The pressure drop inside the NETmix increases since a slurry of hydrates is now flowing inside the network of chambers and channels. This slurry is more viscous than water, thus the pressure drop increases.

While initially, the fluids flowing inside the NETmix network were being cooled by the cooling plates and coolant flowing inside, once hydrate starts to be produced, a significant amount of heat not removed by the cooling fluid is produced. This is detected by the increase of the temperature at the outlet of the NETmix device once hydrate is being formed. Nevertheless, despite these disturbances, the unit was able to keep the temperature within hydrate formation conditions, and thus allowing continuous production, as shown in Figure 6.4.

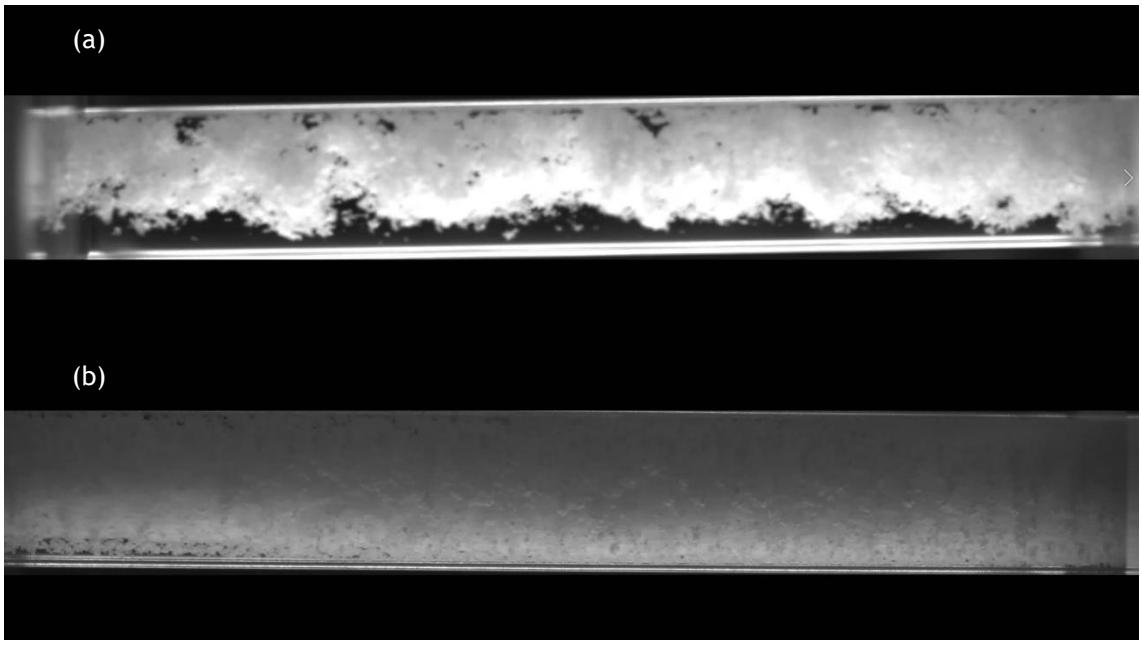

Figure 6.4: (a) Beggining of hydrate formation; (b) fully developed hydrate slurry

6.2 Continuous CO_2 + THF hydrate Production

For a second series of runs, a thermodynamic promoter, tetrahydrofuran, or THF, was added to the water stream, and simultaneously in the NETmix with CO_2. The objective is to assess the impact the THF has on the hydrate formation conditions, that are milder, and, consequently, should favour the continuous production even further.

While in the first set of experiments, water was continuously fed using a system that includes the automatic filling of the water tank with tap water, in this set of experiments, the mixture of THF in water is rerouted and recycled to the vessel where it is mixed to eliminate the need to produce large amounts of the mixture and waste organic compound.

The operating conditions of the experiment are in Table 6.2.

Table 6.2: Conditions for continuous CO_2+THF hydrate production experiments

Run	*Pressure* / bar	*Temperature* / ^{0}C	*Water flow rate* / kg·h^{-1}	*CO2 flow rate* / kg·h^{-1}	*THF concentration* (% mol)
R-24	5	2,8 - 3,2	10	1	0,1%
R-25	10	2,5 - 3	10	1	0,1%
R-26	15	2,5 - 3	10	1	0,1%
R-27	20	2,5 - 3,5	10	1	0,1%
R-28	30	3	10	1	0,1%
R-29	5	2,5 - 3	10	1	0,5%
R-30	10	2- 3	10	1	0,5%
R-31	15	2,5 - 3	10	1	0,5%
R-32	20	2 - 2,8	10	1	0,5%
R-33	30	2,5 - 3	10	1	0,5%

The rate of success for hydrate formation was higher for this set of experiments, since R-27, R-28, R-30, R-31, R-32 and R-33 were able to successfully form hydrates. Figure 6.5 shows the telemetry for R-28 where hydrates were formed.

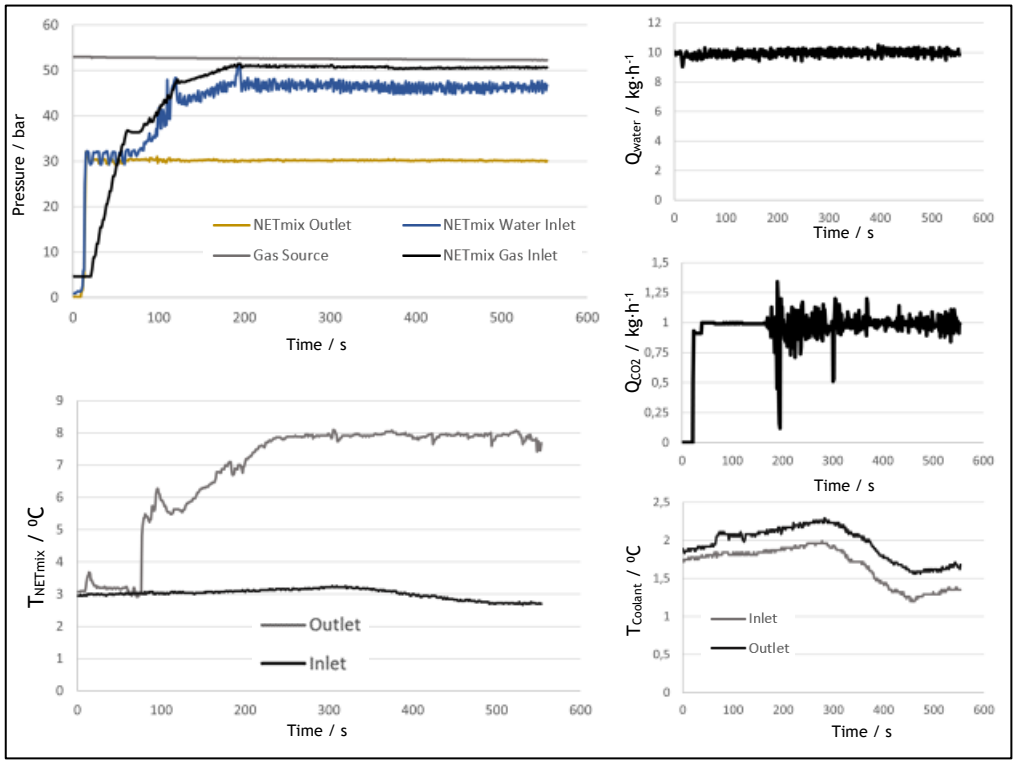

Figure 6.5: Telemetry from run R-28

Although most parameters remained stable, the higher increase of the gas pressure, when compared to the experiments with pure CO_2, made the CO_2 injection less stable. The differences in the outlet and inlet temperatures in the NETmix also increased if compared to when no THF is present. Nevertheless, even though the temperature increased to 8 ºC and pressure drop was higher (see Figure 6.6), the continuous production of hydrates was still possible.

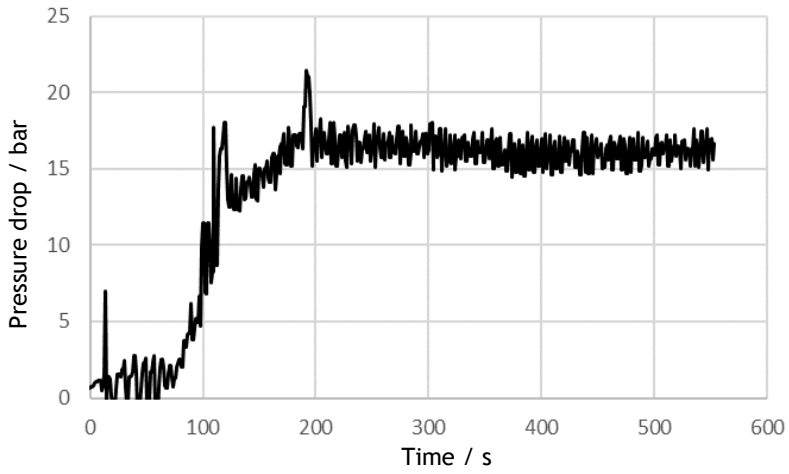

Figure 6.6: Pressure drop in the Netmix for R-28

Even though water flow rate is halved, when compared with R-10, it was expected that the difference between inlet and outlet temperature remained quite similar since the rate of hydration was also halved. However that was not the case since a 5ºC increase was observed, and when compared to the 3ºC increase in the first set of experiments, we can conclude that the heat released is superior when hydrates are formed with CO_2 and THF for 0.1% molar of THF. This increase in hydration heat was expected given that it is supported by the literature from studies like those by Kang et all. (2001), Sabil et al.(2010) and Lirio et al. (2013) in which adding increasingly higher concentrations of THF provided higher hydration heat, which doubled for concentrations of 1-3% mol of THF.

In spite of the fact that the thermodynamic promoter proved to further allow the unit to easily produce hydrates, when the concentration reached 0,5% mol and for pressures above 10 bar, the recycled THF solution formed a foam in the storage vessel, which is undesired since it may damage the pump. The impact of this foam can be detected in the telemetry, in the form of a low-intensity noise in the water flow rate. Therefore, the experiments with 0.5% mol of THF had to be immediately stopped once hydration formation started (see Appendix B.2) and only the ones with 0,1% mol provided useful data.

6.3 Gravimetry Analysis

To extract a hydrate sample, the outlet stream of the NETmix is rerouted to a vessel (H-E-3) to be detached from the unit and stored in the freezer when filled, to keep the extracted sample in a metastable condition, for a 24h period.

Before sample extraction a drastic pressurization was performed at the beginning of a test run and hydrates were formed. When the conditions were shifted back to those of runs which had not formed hydrates, the continuous production would carry on. This happens since a “memory effect” phenomenon allows hydrate to form more easily from gas and water obtained by melting hydrate, than from fresh water with no previous hydrate history[14]. In the case of a reactor the hydrate nuclei, not visible to the naked eye, will remain in its walls and promote the start of hydrate formation.

Therefore, several runs from the previous set of experiments, with different conditions, were handpicked to be collected and to estimate the gas uptake of the formed hydrate.

Since experiments using THF were not as stable, samples with both CO_2 and THF were not analyzed.

The conditions of formation of the hydrate’s samples extracted are presented in Table 6.3:

Table 6.3: Conditions for CO_2 hydrate sample extraction from continuous production

Sample	*Pressure* / bar	*Temperature* / ºC	*Water flow rate* / kg·h^{-1}	*CO2 flow rate* / kg·h^{-1}
S-1 (R-3)	20	2-3	10	1
S-2 (R-11)	20	2-3	20	2
S-3 (R-14)	30	2-3	10	1
S-4 (R-22)	30	2-3	20	1,5

After cooling the sample in the freezer, the vessel is slightly heated using tap water on its surface, allowing the sample removal. The sample is then placed in a weighing scale to measure the evolution of the mass decrease, while the trapped CO_2 leaks from the vessel, since gas will leave the sample through gasification. The obtained gasification curves for each sample are presented in Figure 6.7 and the main results in Table 6.4.

Table 6.4: Data from gravimetric analysis for C02 hydrate sample

Sample	*Initial weight* / g	*Final weight* / g	*CO2 amount* (wt%)	*Hydration number* (n_h)
S-1	5,90	5,11	13,3%	15,9
S-2	20,84	17,97	13,7%	15,4
S-3	12,79	11,83	7,5%	30,2
S-4	14,48	12,41	14,3%	14,7

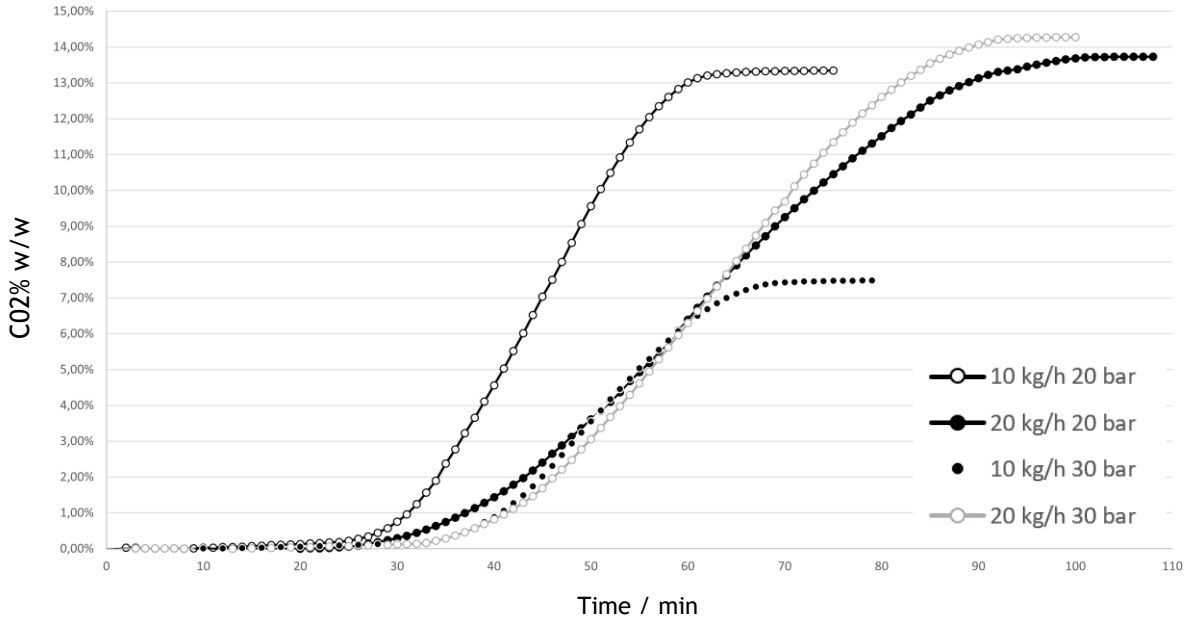

Figure 6.7: CO_2 relase upon hydrate dissociation

The time required for the complete gasification and release of CO_2 can be noted to be dependent on the weight of the sample. This happens because for every sample the maximum carbon dioxide release rate is 0,3% w/w per minute, meaning that higher total mass or CO_2 amount does not provide higher release rates.

There seems to be no direct relation between the amount of CO_2 and either pressure or water flow rate. Nevertheless, the unit and method applied enable the production of hydrates with CO_2 %w/w between 13 and 14% with some degree of consistency.

The hydration numbers obtained, although consistent, are still far from the theoretical value of 7,6, from Equation 1.2. Using NETmix technology Costa (2017) has been able to produce hydrates with an hydration number up to 11, which translates into about 18%CO_2 w/w. To obtain better results, one should alter the extraction method, since sample manipulation can significantly reduce the dissociation kinetics, but does not eliminate it completely. One must highlight that the hydrate is at a metastable condition at the temperature of the freezer (near -20 ºC) and ambient pressure, meaning that even when the dissociation is very slow, it still dissociates. When manipulating the sample, it absorbs heat from the environment and gasification kinetics increases, even before the sample is placed in the scale. This means that when the measurement starts, already a significant amount of gas has fled the sample.

7 Conclusions

The main goal of the present work was initiate the studies and evaluate the performance of a new microscale unit for continuous hydrate production for CO2 separation from exhaust gases, using the NETmix technology.

Studies of heat and mass transfer performance were performed to better understand the advantage of using the NETmix technology for HGtS when compared to other separation technologies. CO2 hydrates were continuously produced to evaluate the system ability to carry out the process as well as study the properties of the hydrates obtained.

In Chapter 4, heat transfer performance was studied for both NETmix in the unit and was concluded that both operate at similar conditions, as expected, with overall heat transfer coefficient ranging from 200 $W \cdot m^{-2} \cdot {}^{o}C^{-1}$ for a Reynolds number of 80, to 4000 $W \cdot m^{-2} \cdot {}^{o}C^{-1}$ for a Reynolds number of 1250. For a Reynolds number superior to 800, the NETmix network heat transfer resistance becomes smaller than all the other resistances in the system.

Mass transfer performance tests were carried out, in Chapter 5, and the unit proved to have volumetric mass transfer coefficients ranging from 1700 h^{-1} for a Reynolds number of 264, to 8000 h^{-1} for a Reynolds number of 661. The values obtained revealed to be far superior to other gas-liquid mass transfer equipment.

Hydrate formation for both CO_2 and CO_2+THF hydrates was achieved successfully in Chapter 6. It can be stated with certainty that hydrates were formed, and not ice, since the temperature conditions on the NETmix were always kept above 0 ^{o}C. For CO_2 hydrates, it was determined that higher pressure and higher water flow rate promoted an easier formation. For CO_2+THF hydrates, its formation proved to be fairly easier to achieve when compared to hydrates without the thermodynamical promoter. The amount of heat released by the formation of hydrates containing THF was larger than those only containing CO_2. The unit was able to isolate CO_2 hydrate samples which upon further gravimetric analysis presented some degree of consistency in forming structures with hydration numbers ranging from 14,7 to 15,9 which represents about 13,3-14,3% in CO_2 w/w.

7.1 Recommendations

Although this work was carried out without any major obstacles to the unit performance, some improvements and studies can be suggested to further maximize the unit capability for future experiments.

Regarding heat transfer, to fully understand the amount of heat released during hydrate formation, overall heat coefficient studies with hydrate slurry flow can prove useful since all temperatures are always known at every moment of production.

The THF addition to the system should be carried out by using an auxiliar pump, which would hinder the formation of foam and prevent the pump from being damaged. This should make production of hydrates with concentrations of THF higher than 0,1% mol safe and achievable.
Lastly, the method for extracting samples has to be redesigned. Large amounts of CO_2 are lost when the vessel containing the sample is heated for extraction, which means that the results obtained will never reach the higher hydration numbers expected. The solution might be to collect the samples in a vessel that can be weighed, thus removing the necessity of extracting the sample, either by adding heat or by using an invasive mechanical method.
Nevertheless, the P01 is definitely promising in performing CO_2/N_2 separation using the HGtS technology, which should be the next step.

8 References

[1]. Song, C., Liu, Q., Deng, S., Li, H. and Kitamura, Y., 2019. Cryogenic-based CO2 capture technologies: State-of-the-art developments and current challenges. *Renewable and Sustainable Energy Reviews*, 101, pp.265-278.

[2]. IPCC, Masson-Delmotte, V., P. Zhai, H.-O. Pörtner, D. Roberts, J. Skea, P.R. Shukla, A. Pirani, W. Moufouma-Okia, C. Péan, R. Pidcock, S. Connors, J.B.R. Matthews, Y. Chen, X. Zhou, M.I. Gomis, E. Lonnoy, T. Maycock, M. Tignor, and T. Waterfield (eds.), 2018. Summary for Policymakers. In: Global Warming of 1.5°C. An IPCC Special Report on the impacts of global warming of 1.5°C above pre-industrial levels and related global greenhouse gas emission pathways, in the context of strengthening the global response to the threat of climate change, sustainable development, and efforts to eradicate poverty.

[3]. Lovett, J., Hofman, P., Morsink, K., Torres, A., Clancy, J. and Krabbendam, K., 2009. Review of the 2008 UNFCCC meeting in Poznań. Energy Policy, 37(9), pp.3701-3705.

[4]. United Nations Environment Programme, 2021. Letter from the Executive Director. Annual Report. [online] Available at: <https://wedocs.unep.org/bitstream/handle/20.500.11822/34917/AN2020.pdf?sequence=3&isAllowed=y> [Accessed 20 September 2021].

[5]. Fawzy, S., Osman, A., Doran, J. and Rooney, D., 2020. Strategies for mitigation of climate change: a review. *Environmental Chemistry Letters*, 18(6), pp.2069-2094.

[6]. Lee, S. and Park, S., 2015. A review on solid adsorbents for carbon dioxide capture. *Journal of Industrial and Engineering Chemistry*, 23, pp.1-11.

[7]. Olivier, J., Bouwman, A., van der Maas, C. and Berdowski, J., 1994. Emission database for global atmospheric research (Edgar). *Environmental Monitoring and Assessment*, 31-31(1-2), pp.93-106.

[8]. Leung, D., Caramanna, G. and Maroto-Valer, M., 2014. An overview of current status of carbon dioxide capture and storage technologies. *Renewable and Sustainable Energy Reviews*, 39, pp.426-443.

[9]. IEA, 2016. *20 years of carbon capture and storage*, IEA Publications, Paris https://www.iea.org/reports/20-years-of-carbon-capture-and-storage accessed September 20, 2021

[10]. Costa, M.F. 2017. The NETmix® Technology, Applied to Gas Hydrates Production: A Potential Solution to CCS [Ph.D Thesis]. Porto, Portugal: Departamento de Engenharia Química, Universidade do Porto.

[11]. IEA, 2019. World Energy Model; Scenario analysis of future energy trends. International Energy Agency. https://www.iea.org/reports/world-energy-model/sustainable-development-scenario: accessed September 20, 2021

[12]. Rackley, S., 2010. *Carbon capture and storage*. Burlington: Butterworth-Heinemann.

[13]. Wang Y. Zhao L. Otto A. et al. (2017), A review paper of post-combustion CO2 capture technologies from coal-fired power plants. Energy Procedia vol. 114, July 2017, 650-665. https://doi.org/10.1016/j.egypro.2017.03.1209

[14]. Parker, Larry; Stine, Deborah D. & Folger, Peter. Capturing CO2 from Coal-Fired Power Plants: Challenges for a Comprehensive Strategy, report, February 13, 2009; Washington D.C.. (https://digital.library.unt.edu/ark:/67531/metadc743641/: accessed September 20, 2021), University of North Texas Libraries, UNT Digital Library, https://digital.library.unt.edu; crediting UNT Libraries Government Documents Department.

[15]. Smit, B., 2014. *Introduction to carbon capture and sequestration*. London: Imperial College Press.

[16]. Buhre, B., Elliott, L., Sheng, C., Gupta, R. and Wall, T., 2005. Oxy-fuel combustion technology for coal-fired power generation. *Progress in Energy and Combustion Science*, 31(4), pp.283-307.

[17]. IPCC, 2014: *Climate Change 2014: Synthesis Report. Contribution of Working Groups I, II and III to the Fifth Assessment Report of the Intergovernmental Panel on Climate Change* [Core Writing Team, R.K. Pachauri and L.A. Meyer (eds.)]. IPCC, Geneva, Switzerland, 151 pp.

[18]. Burdyny, T. and Struchtrup, H., 2010. Hybrid membrane/cryogenic separation of oxygen from air for use in the oxy-fuel process. *Energy*, 35(5), pp.1884-1897.

[19]. Global CCS Institute, 2012. CO2 capture technologies: oxy combustion with CO2 capture

[20]. Martinho, A.R. 2020. Life cycle assessment of a novel CO2 Capture Technology (HGtS) on retrofitting coaol and natural gas power platns: Portugal case study. Porto, Portugal: Departamento de Engenharia do Ambiente, Universidade do Porto.

[21]. Prah, B. and Yun, R., 2018. CO2 hydrate slurry transportation in carbon capture and storage. *Applied Thermal Engineering*, 128, pp.653-661

[22]. He, J., Liu, Y., Ma, Z., Deng, S., Zhao, R. and Zhao, L., 2017. A Literature Research on the Performance Evaluation of Hydrate-based CO 2 Capture and Separation Process. *Energy Procedia*, 105, pp.4090-4097.

[23]. Englezos, P. and Lee, J., 2005. Gas hydrates: A cleaner source of energy and opportunity for innovative technologies. *Korean Journal of Chemical Engineering*, 22(5), pp.671-681.

[24]. Carroll, J., 2010. *Natural Gas Hydrates, 3rd Edition*.

[25]. Taylor, C., 2010. *Advances in the study of gas hydrates*. New York: Springer.

[26]. Sloan, E. and Koh, C., 2007. *Clathrate hydrates of natural gases*. Boca Raton, FL: CRC Press/Taylor & Francis.

[27]. Kang, S., Lee, H., Lee, C. and Sung, W., 2001. Hydrate phase equilibria of the guest mixtures containing CO2, N2 and tetrahydrofuran. *Fluid Phase Equilibria*, 185(1-2), pp.101-109.

[28]. Dashti, H., Zhehao Yew, L. and Lou, X., 2015. Recent advances in gas hydrate-based CO2 capture. *Journal of Natural Gas Science and Engineering*, 23, pp.195-207.

[29]. Linga, P., Haligva, C., Nam, S., Ripmeester, J. and Englezos, P., 2009. Gas Hydrate Formation in a Variable Volume Bed of Silica Sand Particles. *Energy & Fuels*, 23(11), pp.5496-5507.

[30]. Ma, Z., Zhang, P., Bao, H. and Deng, S., 2016. Review of fundamental properties of CO 2 hydrates and CO 2 capture and separation using hydration method. *Renewable and Sustainable Energy Reviews*, 53, pp.1273-1302.

[31]. Delahaye, A., Fournaison, L., Marinhas, S., Chatti, I., Petitet, J., Dalmazzone, D. and Fürst, W., 2006. Effect of THF on Equilibrium Pressure and Dissociation Enthalpy of CO2Hydrates Applied to Secondary Refrigeration. *Industrial & Engineering Chemistry Research*, 45(1), pp.391-397.

[32]. Linga, P., Kumar, R., Lee, J., Ripmeester, J. and Englezos, P., 2010. A new apparatus to enhance the rate of gas hydrate formation: Application to capture of carbon dioxide. *International Journal of Greenhouse Gas Control*, 4(4), pp.630-637.

[33]. Linga, P., Kumar, R. and Englezos, P., 2007. The clathrate hydrate process for post and pre-combustion capture of carbon dioxide. *Journal of Hazardous Materials*, 149(3), pp.625-629.

[34]. Li, R., Li, X., Chen, Z., Zhang, Y., Xu, C. and Xia, Z., 2018. Anti-Agglomerator of Tetra-n-Butyl Ammonium Bromide Hydrate and Its Effect on Hydrate-Based CO2 Capture. *Energies*, 11(2), p.399.

[35]. Fonte, C., Leblebici, M., Dias, M. and Lopes, J., 2013. The NETmix reactor: Pressure drop measurements and 3D CFD modeling. *Chemical Engineering Research and Design*, 91(11), pp.2250-2258.

[36]. Gomes, P., 2011. *The NETmix® Reactor: Strategies for Optimizing Miing and Development of New Reactor* [Ph.D Thesis]. Porto, Portugal: Departamento de Engenharia Química, Universidade do Porto.

[37]. Fonte, C., 2013. *The NETmix® Reactor: Application to High Added-Value Products* [Ph.D Thesis]. Porto, Portugal: Departamento de Engenharia Química, Universidade do Porto.

[38]. Laranjeira, P., 2005. NETmix® Static Mixer:Modelling, CFD Simulation and Experimental Characterisation Porto, Portugal: Departamento de Engenharia Química, Universidade do Porto

[39]. Lorenzoni, N., 2020. Computational study of heat exchange in a mesostructured network mixer. Porto, Portugal: Departamento de Engenharia do Ambiente, Universidade do Porto.

[40]. Ribeiro, A., Manrique, Y., Barreiro, F., Lopes, J. and Dias, M., 2021. Continuous production of hydroxyapatite Pickering emulsions using a mesostructured reactor. *Colloids and Surfaces A: Physicochemical and Engineering Aspects*, 616, p.126365.

[41]. Green, D. and Perry, R., 2003. *Perry's chemical engineers' handbook*. New York: McGraw-Hill.

[42]. Welty, J., 2008. *Fundamentals of momentum, heat, and mass transfer*.Wiley.

[43]. Márquez, A., Wild, G. and Midoux, N., 1994. A review of recent chemical techniques for the determination of the volumetric mass-transfer coefficient kLa in gas—liquid reactors. *Chemical Engineering and Processing: Process Intensification*, 33(4), pp.247-260.

Appendix

A Evaluate NETmix individual heat transfer resistances

Once the global heat coefficient *U* for the equipment is known, if there is enough data, it is possible to determine the individual convective resistance for the NETmix side.

From CFD studies carried out by Lorenzoni (2020), a relation between convective heat transfer in the coolant side, $h_{Coolant}$, with increasing flow rate is already established (Figure A.1).

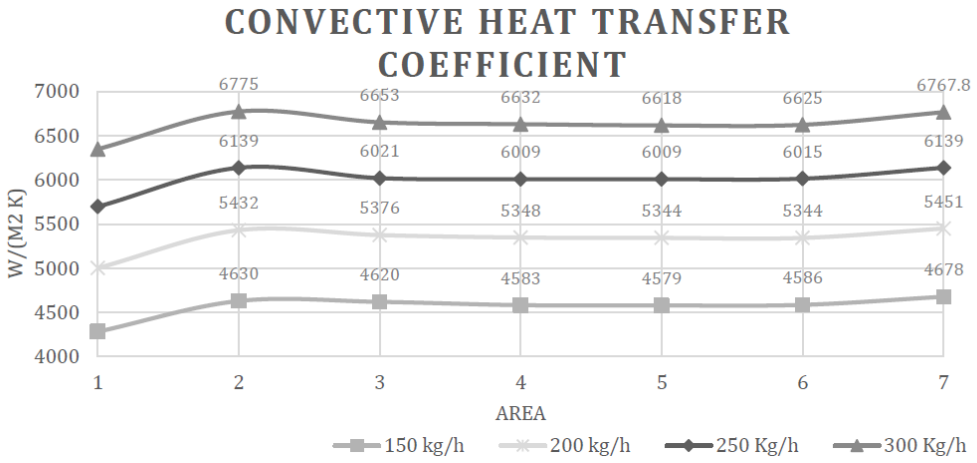

Figure A.1: Coolant side convective heat transfer coefficient along the longitudinal profile for P01 unit (Lorenzoni, 2020)

This data alowed to extrapolate the value for this coefficient to the flow rate used in P01's NETmix reactors. That flow rate is 530 kg·h^{-1} from which was obtained a $h_{Coolant}$ of about 10000 W·m^{-2}·K^{-1}.

To determine the resistance by conduction there needs to be a knowledge of the plate material as well as the distance heat travels thorugh. The plate material is AISI 316 stainless steel which has a thermal condutivity of 16.27 W·m^{-1}·K^{-1}. Figure A.2 provides the thickness of the plate through where heat flows.

With this data, using equation 3.4, h_{NETmix} was calculated.

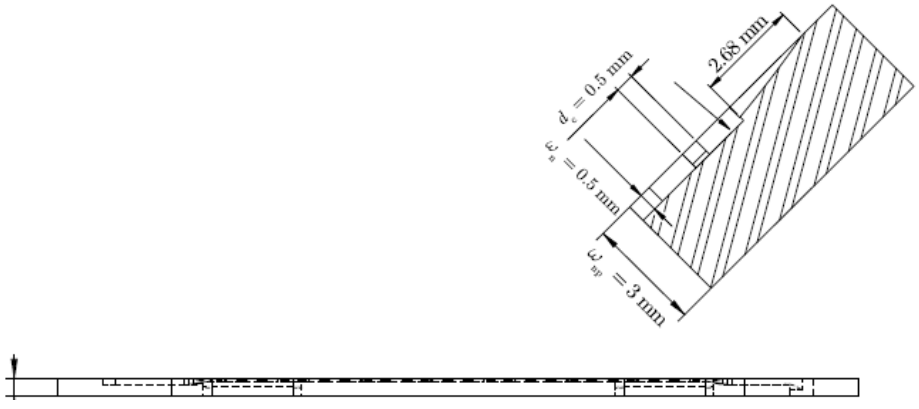

Figure A.2: NETmix lateral view and detail (Costa, 2017)

B Telemetry

B.1 Telemetry for CO_2 Hydrates Continuous Production

The telemetries for runs R-14 and R-20 (Figure B.1 and B.2 respectively) further evidence the pattern observed when hydrates are produced.

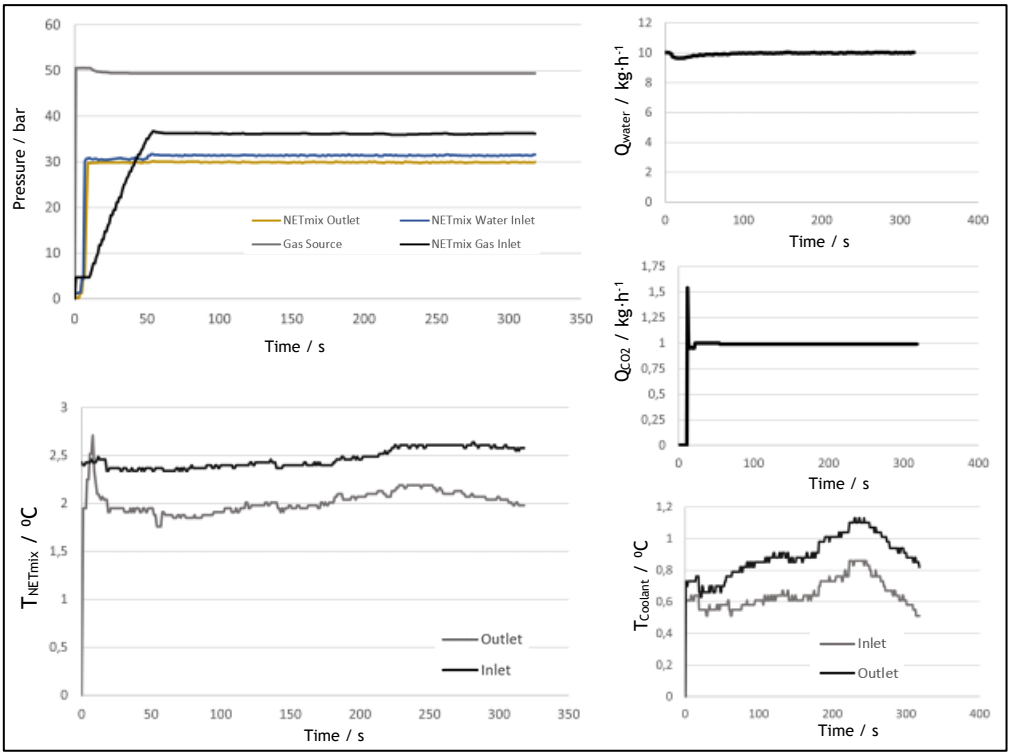

Figure B.3: Telemetry for R-14

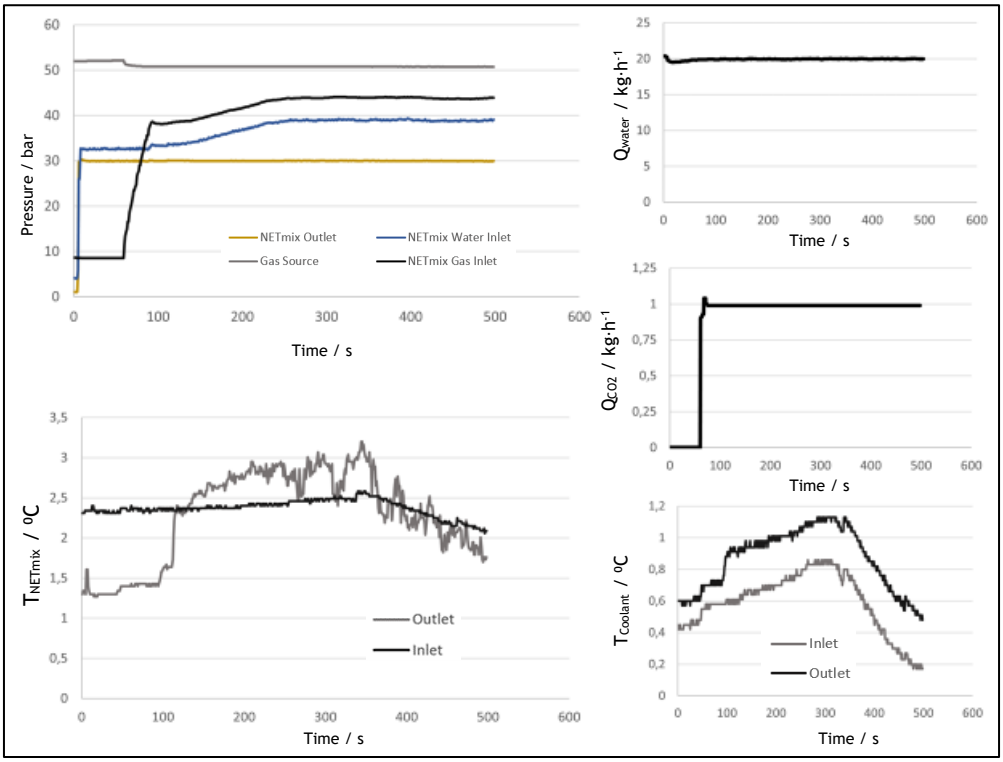

Figure B.4: Telemetry for R-20

As seen in Chapter 6, when hydrates are formed the coolant outlet temperature doubles, the NETmix outlet temperature suffers a drastic increase and the pressure inside the reactor also gets increasingly higher. In Figure B.4, where hydrates were succesfully produced, the increase of 3ºC temperature at the NETmix outlet is similar to R-22 (see Figure 6.2) which should represent a similiar hydration heat observed.

B.2 Telemetry for CO_2 + THF(0,5% mol) Hydrates Continuous Production

The telemetry for run R-32 in Figure B.3 shows the pressure spike and noise in the mass flow controllers that prevent the continuous hydrate production 0,5% mol THF to be carried out.

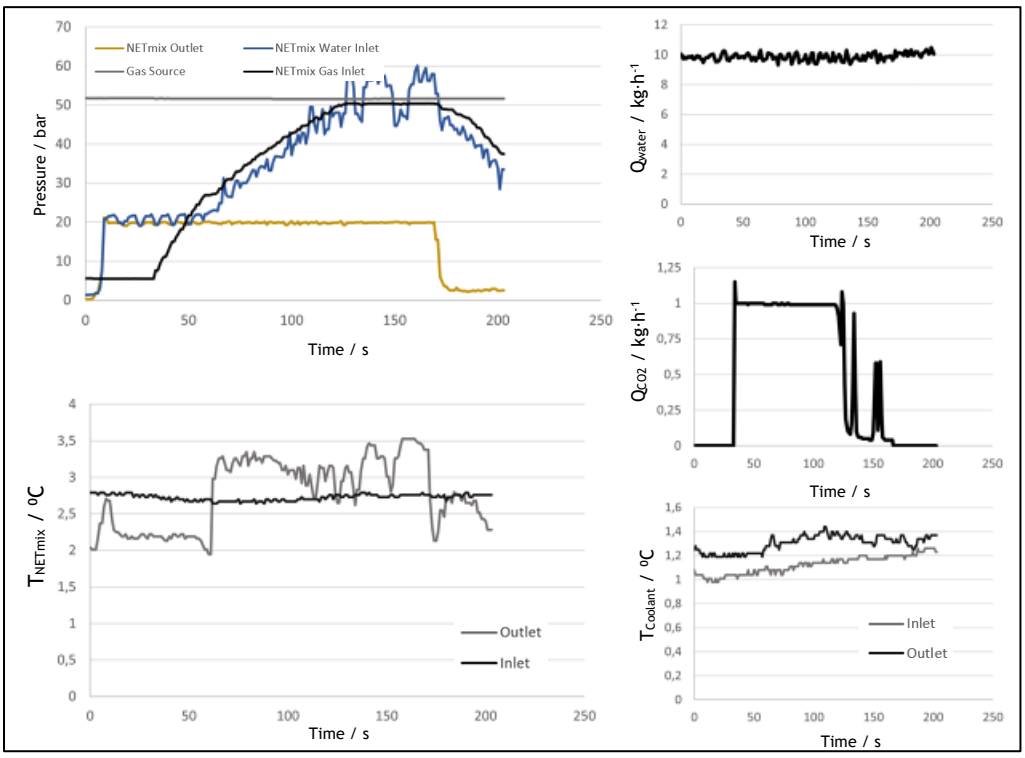

Figure B.5: Telemetry for R-32

As it can be observed, as soon as hydrates formed, the pressure increased to levels higher than the gas source which prevented gas to keep flowing and carrying on the experiment could damage the whole unit.